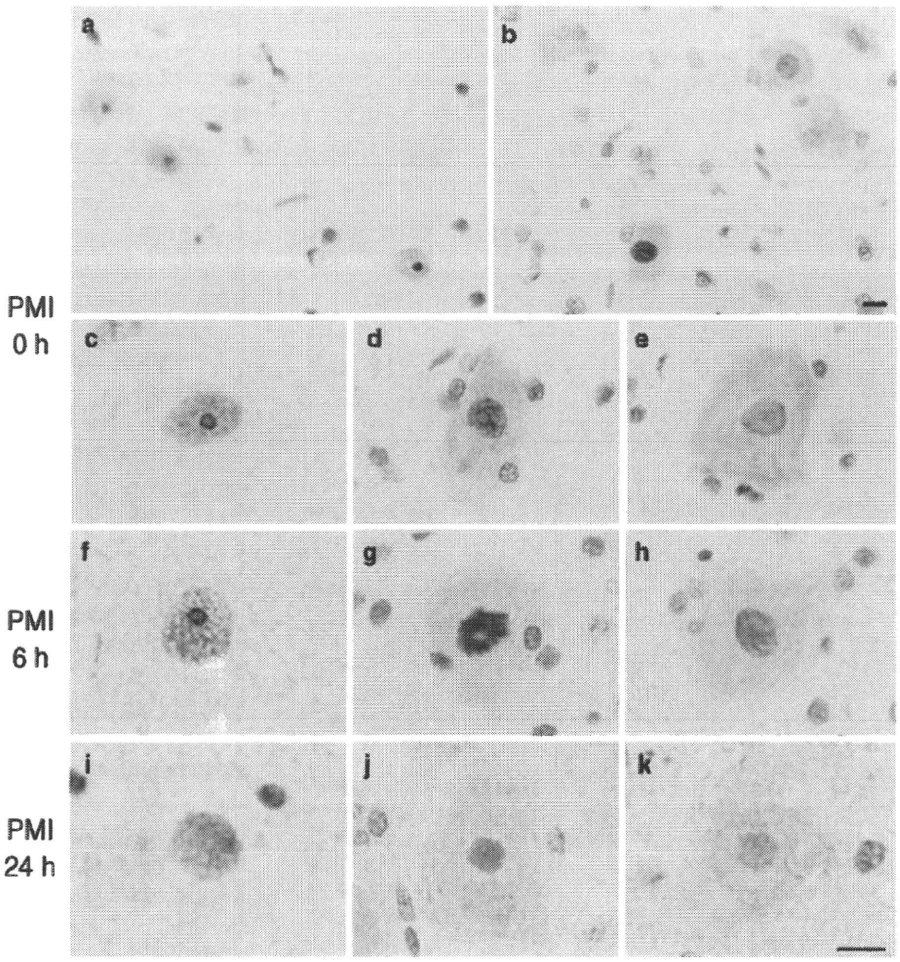

Fig. 2 ADAR2 immunohistochemistry of motor neurons in the rat lumbar spinal cord. ADAR2 is expressed in the nuclei of neurons in frozen sections created at 0 h postmortem (**a**, **c**). On the contrary, ADAR2 is always positive in the cytoplasm of neurons in formalin-fixed, paraffin-embedded sections from different rats, with a variable intensity of nuclear immunoreactivity among neurons (**b**, **d**, **e**). Frozen (**f**) and paraffin-embedded sections (**g**, **h**) with a 6-h postmortem interval display immunoreactivity similar to those with a 0-h postmortem interval. Nuclear immunoreactivity was less intense on both frozen sections (**i**) and paraffin-embedded sections (**j**, **k**) created at 24 h postmortem compared with those prepared at 0 h. *PM* postmortem interval. *Bar* indicates 20 μm

neurons (Figs. 4a′, a″, b′, 5b, c), while phosphorylation-dependent TDP-43 (pTDP-43) did not stain either the nucleus or cytoplasm on the adjacent section (Fig. 4b″). Two different anti-ADAR2 antibodies exhibited immunoreactivity in the cytoplasm of motor neurons (Fig. 4a, b, g, Supplementary Figure 2), and preabsorbed anti-ADAR2 antibody did not show any immunoreactivity (Fig. 4h).

ADAR2, pTDP-43 and piTDP-43 expression in ALS spinal motor neurons

Both ADAR2-positive (Fig. 4c open arrow) and -negative motor neurons (Fig. 4c closed arrow) were observed in the ALS spinal cords. The immunoreactivity in the ADAR2-positive neurons was observed in the cytoplasm, but apparently not in the nuclei (Figs. 4c open arrow, e, f, 5d, f), as observed in the control motor neurons. These ADAR2-positive neurons showed normal piTDP-43 immunoreactivity in the nucleus (Figs. 4e′, f′, 5e, f,), but exhibited no pTDP-43-positive inclusions (Fig. 4c, c′). In contrast, all ADAR2-negative neurons showed pTDP-43-positive inclusions in the cytoplasm (Fig. 4c′, d′).

Cell count of anterior horn motor neurons

The number of anterior horn cells (motor neurons) (AHC) in 7 sporadic ALS cases was reduced to 39 ± 21% (mean ± SD) of the number in control cases ($p < 0.0001$, Mann–Whitney's U test, Fig. 6). A significant proportion of motor neurons (98 out of 170 anterior horn cells; 58%) in the spinal cords obtained from patients with ALS were ADAR2-negative (Table 1; Fig. 6). ADAR2-negative motor neurons were observed in all ALS cases examined, but the proportions varied from 30% in case 3 to 100% in case 2 (Table 1). Notably, all the ADAR2-negative motor neurons had pTDP-43-positive inclusions in the cytoplasm. Conversely, virtually all the ADAR2-positive motor neurons had piTDP-43 immunoreactivity in their nuclei, but did not exhibit pTDP-43-positive cytoplasmic inclusions (Table 1; Fig. 6). Only one motor neuron was stained with

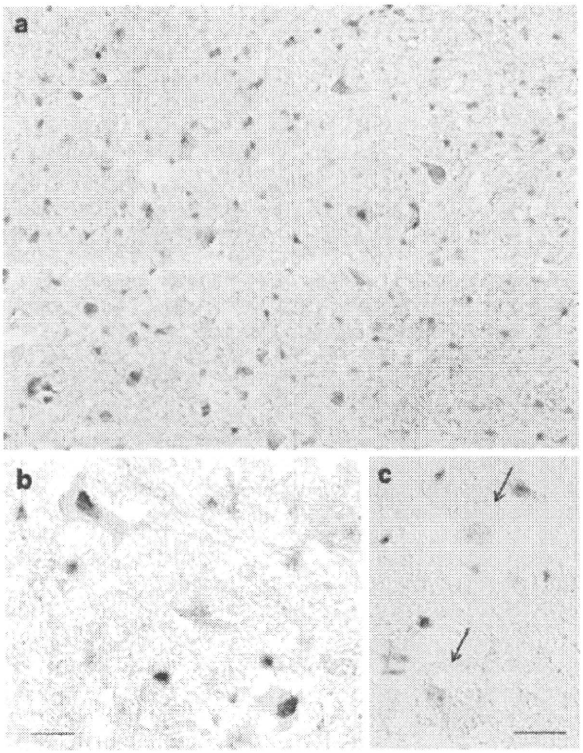

Fig. 3 Expression of ADAR2 and phosphorylation-dependent TDP-43 in spinal motor neurons of SOD1 transgenic mice. A low-magnification view of the lumbar spinal anterior horn in a $SOD1^{G93A}$ transgenic mouse, at 34 weeks of age showing that all the motor neurons are ADAR2 positive (**a**). A high-magnification view shows predominant nuclear immunoreactivity (**b**). There is no phosphorylation-dependent TDP-43 immunoreactive inclusion in the motor neurons (**c**, *arrow*). *Bar* indicates 20 μm

both ADAR2 and pTDP-43 ($n = 1$ in case 4), but none of the motor neurons lacked immunoreactivity to both ADAR2 and pTDP-43. These results indicate a strong association between ADAR2-deficiency and the development of pTDP-43-positive inclusions in the motor neurons of patients with sporadic ALS. However, there is no apparent relationship between the duration of disease and the number of remaining motor neurons with ADAR2 positivity and/or pTDP-43 positivity.

Discussion

ADAR2 expression was observed in all 380 spinal motor neurons examined in the control cases in this study, and in a portion of the spinal motor neurons from ALS cases (approximately 42% of 170 neurons). The nuclei of these ADAR2-positive neurons were also immunoreactive for piTDP-43. Notably, more than half the motor neurons in ALS cases lacked immunoreactivity to both ADAR2 and piTDP-43, but these double-negative neurons always displayed pTDP-43-positive inclusions in the cytoplasm. Therefore, normal motor neurons express ADAR2 without forming phosphorylated TDP-43-positive cytoplasmic inclusions, whereas motor neurons lacking ADAR2 in sporadic ALS formed inclusions.

ADAR2 immunoreactivity was exclusively observed in the nuclei of rat motor neurons on the frozen sections created 0–6-h postmortem. Because the density of motor neurons in the spinal ventral gray matter is too low to detect ADAR2 by Western blotting analysis, we used frozen human brain for the analysis, which demonstrated that RED1 specifically recognized two isoforms of active ADAR2 protein in the nuclear fraction [17]. The nuclear localization of the ADAR2 protein in the motor neurons was demonstrated immunohistochemically in frozen human spinal cord sections. In addition, expression of ADAR2 mRNA in the human spinal cord was demonstrated [18]. These results are consistent with the function of ADAR2 in the cell nucleus, which is catalysis of the conversion of adenosine to inosine (A-to-I) at various pre-mRNA positions including the Q/R site of GluR2. We also observed ADAR2 immunoreactivity in the cytoplasm of motor neurons in human paraffin-embedded sections. Importantly, the nuclei of motor neurons were predominantly immunoreactive to ADAR2 in frozen sections of the same control subject. In paraffin-embedded sections and frozen sections from the spinal cord after a 24-h postmortem interval, there was a reduction in ADAR2 immunoreactivity in the nucleus with the concomitant appearance of immunoreactivity in the cytoplasm of rat motor neurons. Therefore, ADAR2 immunoreactivity in the cytoplasm likely represented ADAR2 protein translocated from the nucleus to the cytoplasm resulting from the procedure of paraffin embedding and/or the delay between death and tissue fixation, which are unavoidable during routine neuropathological examinations of human autopsy materials. Because all the control motor neurons demonstrated cytoplasmic ADAR2 immunoreactivity, it is likely that ADAR2-negative motor neurons in ALS spinal cords lacked ADAR2 protein localized to the nucleus.

ADAR2 is involved in the A-to-I conversion of various pre-mRNAs and specifically catalyzes GluR2 Q/R site-editing. AMPA receptors containing GluR2 which is unedited at the Q/R site have significantly higher Ca^{2+} permeability than those containing edited GluR2. This factor plays a crucial role in neuron survival [5, 31]. Neurons in the mammalian brain only express Q/R site-edited GluR2 mRNA, and mice unable to edit this site die from status epilepticus early in life [14]. GluR2 Q/R site-editing occurs with 100% efficiency in normal human motor neurons, but is characterized by high variability (from 0 to 100%) among individual motor neurons in individual cases of ALS [16]. Therefore, ADAR2-positive

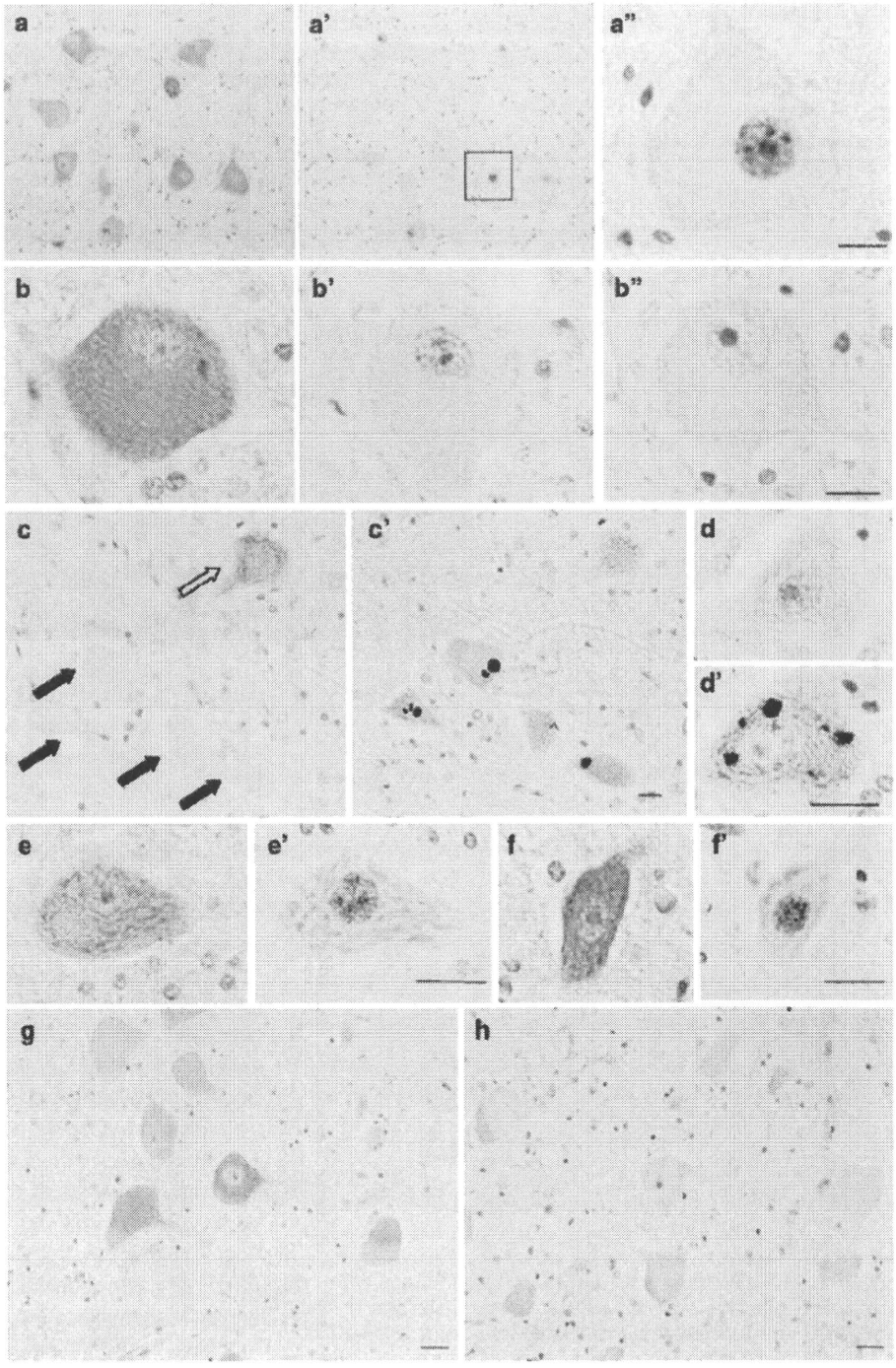

Fig. 4 Expression of ADAR2, phosphorylation-dependent TDP-43 and phosphorylation-independent TDP-43 in spinal motor neurons from adjacent sections. A low-magnification view of the lumbar spinal anterior horn in a control subject (case 8) shows that all the motor neurons are immunoreactive for ADAR2 (**a**). These neurons show phosphorylation-independent TDP-43 (piTDP-43) immunoreactivity in the nucleus in an adjacent section (**a′**, **a″**: a high-magnification view of the open square in **a′**). A lumbar spinal motor neuron from a control subject (case 12) shows diffuse ADAR2 immunoreactivity in the cytoplasm (**b**). The adjacent section shows piTDP-43 immunoreactivity in the nucleus (**b′**), but does not show phosphorylation-dependent TDP-43 (pTDP-43) immunoreactivity (**b″**). All ADAR2-negative neurons (*closed arrows* in *c*; case 6) display pTDP-43-positive inclusions in the cytoplasm (**c′**), whereas an ADAR2-positive neuron from a patient with ALS (*open arrow* in **c**) has no pTDP-43 immunoreactivity (**c′**). An ADAR2-negative neuron (**d**; case 6) has multiple pTDP-43-positive inclusions in the cytoplasm (**d′**). ADAR2-positive neurons (**e** case 6, **f** case 3) show phosphorylation-independent TDP-43 immunoreactivity in the nucleus (**e′**, **f′**). ADAR2 immunoreactivity in the cytoplasm (**g**) disappeared when recombinant ADAR2-preabsorbed anti-ADAR2 antibody was used as the primary antibody (**h**) (case 12). *Bar* indicates 20 μm

motor neurons likely represent normal neurons expressing Q/R site-edited GluR2, whereas ADAR2-negative motor neurons represent those expressing Q/R site-unedited GluR2 [16, 20]. The present results indicating the presence of both ADAR2-positive and -negative motor neurons are consistent with high variability in the efficiency of GluR2 Q/R site-editing (from 0 to 100%) among individual motor neurons in ALS patients [16]. These findings strengthen the hypothesis that reduced ADAR2 activity is closely associated with the pathogenesis of sporadic ALS [20].

The presence or absence of ADAR2 immunoreactivity in the cytoplasm of motor neurons was conversely related to pTDP-43 immunoreactivity in the cytoplasm. Abnormally processed TDP-43 was initially identified as a

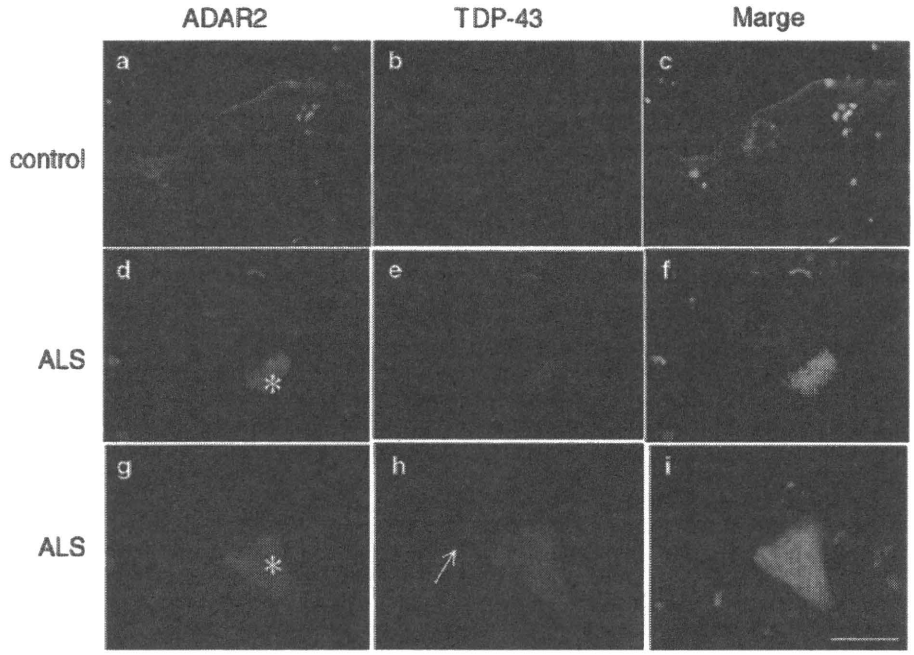

Fig. 5 Double-labeled immunofluorescence study using anti-ADAR2 and anti-piTDP-43 antibodies. **a–c** Control motor neuron was immunopositive for ADAR2 in the cytoplasm and nucleus and piTDP-43 in the nucleus. **d–f** An ALS motor neuron immunoreactive to ADARA2 in the cytoplasm showed immunoreactivity to piTDP-43 in the nucleus. **g–i** An ALS motor neuron lacking immunoreactivity to ADAR2 showed piTDP-43 positive cytoplasmic inclusions (*arrow*) and loss of piTDP-43 immunoreactivity in the nucleus. Asterisks indicate lipofuscin autofluorescence. *Bar* indicates 20 μm

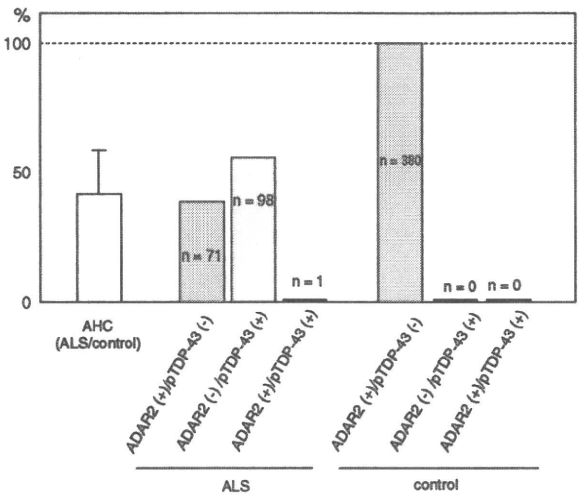

Fig. 6 Motor neurons with different immunoreactivities in ALS and control cases. The number of anterior horn cells (motor neurons) (AHCs) in 7 sporadic ALS cases was reduced to 39 ± 21% (mean ± SD) of the number in control cases ($p < 0.0001$, Mann–Whitney *U* test). In ALS cases, 42% of total AHCs were ADAR2-positive and pTDP-43-negative (*pink bar*); 58% were ADAR2-negative and pTDP-43-positive (*blue bar*). Only one AHC out of 170 (0.2%) was positive for both ADAR2 and pTDP-43, and none were negative for both ADAR2 and pTDP-43. All lumbar spinal motor neurons ($n = 380$) from 6 control cases were ADAR2-positive and pTDP-43-negative (*pink bar*). *AHC* anterior horn cell (motor neuron)

protein component of ubiquitin-positive and tau-negative inclusions in the brains of patients with FTD and ALS [3, 25]. Subsequently, abnormal TDP-43-positive inclusions were found in various proportions in neurons from patients with other neurodegenerative disorders, such as Parkinson's disease dementia and dementia with Lewy bodies [24], Parkinsonism-dementia complex and ALS in Guam [8, 11], corticobasal degeneration [36] and Alzheimer's disease [2, 13, 36]. These results imply that aberrant processing of TDP-43 may be involved in a common pathway of the neurodegenerative process and that the accumulation of pTDP-43 in the cytoplasm of motor neurons is not a disease-specific event in ALS [2, 13, 24, 36].

This study demonstrates that all ADAR2-negative motor neurons showed pTDP-43-positive inclusions in the cytoplasm in cases of sporadic ALS, suggesting a molecular association between reduced ADAR2 activity and the formation of pTDP-43-positive inclusions in ALS motor neurons. Both TDP-43 and ADAR2 are nuclear proteins, playing roles in the regulation of RNA processing; TDP-43 regulates RNA splicing [4, 28] and ADAR2 catalyzes RNA editing. However, there is no report regarding the functional link between the two molecules. We found that pTDP-43-positive inclusions showed no ADAR2 immunoreactivity, indicating that the trapping of ADAR2 protein in the inclusions due to direct protein–protein interaction is unlikely. Reduced ADAR2 activity increases Ca^{2+} permeable AMPA receptors by failure to edit the Q/R site of GluR2 [5, 6, 14], but it is not known whether an increase of the Ca^{2+} overload influences the TDP-43 processing. Thus, it is not clear from the present immunohistochemical study whether the reduced ADAR2 expression is a cause or a consequence of TDP-43 pathology. Interestingly, neither pTDP-43-positive inclusions [23, 35] nor a reduction of GluR2 Q/R-site-editing [19] was associated with

SOD1-related familial ALS or SBMA, an X-linked hereditary lower motor neuron disease associated with expanded CAG repeats in the androgen receptor gene. Consistent with the absence of pTDP-43-positive inclusions in the spinal motor neurons of *SOD1*-associated familial ALS, present study demonstrated that all the motor neurons examined were ADAR2-positive in SOD1^{G93A} transgenic mouse spinal cords. Elucidation of the molecular mechanism underlying the co-occurrence of reduced ADAR2 activity and abnormal TDP-43 pathology in the same motor neurons may provide a clue to the neurodegenerative process of sporadic ALS.

References

1. Akbarian S, Smith MA, Jones EG (1995) Editing for an AMPA receptor subunit RNA in prefrontal cortex and striatum in Alzheimer's disease, Huntington's disease and schizophrenia. Brain Res 699:297–304
2. Amador-Ortiz C, Lin WL, Ahmed Z et al (2007) TDP-43 immunoreactivity in hippocampal sclerosis and Alzheimer's disease. Ann Neurol 61:435–445
3. Arai T, Hasegawa M, Akiyama H et al (2006) TDP-43 is a component of ubiquitin-positive tau-negative inclusions in frontotemporal lobar degeneration and amyotrophic lateral sclerosis. Biochem Biophys Res Commun 351:602–611
4. Buratti E, Baralle FE (2008) Multiple roles of TDP-43 in gene expression, splicing regulation, and human disease. Front Biosci 13:867–878
5. Burnashev N, Monyer H, Seeburg PH, Sakmann B (1992) Divalent ion permeability of AMPA receptor channels is dominated by the edited form of a single subunit. Neuron 8:189–198
6. Carriedo SG, Yin HZ, Weiss JH (1996) Motor neurons are selectively vulnerable to AMPA/kainate receptor-mediated injury in vitro. J Neurosci 16:4069–4079
7. Chen YZ, Bennett CL, Huynh HM et al (2004) DNA/RNA helicase gene mutations in a form of juvenile amyotrophic lateral sclerosis (ALS4). Am J Hum Genet 74:1128–1135
8. Geser F, Winton MJ, Kwong LK et al (2008) Pathological TDP-43 in parkinsonism-dementia complex and amyotrophic lateral sclerosis of Guam. Acta Neuropathol 115:133–145
9. Gitcho MA, Baloh RH, Chakraverty S et al (2008) TDP-43 A315T mutation in familial motor neuron disease. Ann Neurol 63:535–538
10. Hadano S, Hand CK, Osuga H et al (2001) A gene encoding a putative GTPase regulator is mutated in familial amyotrophic lateral sclerosis 2. Nat Genet 29:166–173
11. Hasegeawa M, Arai T, Akiyama H et al (2007) TDP-43 is deposited in the Guam Parkinsonism-dementia complex brains. Brain 130:1386–1394
12. Hasegawa M, Arai T, Nonaka T et al (2008) Phosphorylated TDP-43 in frontotemporal lobar degeneration and amyotrophic lateral sclerosis. Ann Neurol 64:60–70
13. Higashi S, Iseki E, Yamamoto R et al (2007) Concurrence of TDP-43, tau and alpha-synuclein pathology in brains of Alzheimer's disease and dementia with Lewy diseases. Brain Res 1184:284–394
14. Higuchi M, Maas S, Single FN et al (2000) Point mutation in an AMPA receptor gene rescues lethality in mice deficient in the RNA-editing enzyme ADAR2. Nature 406:78–81
15. Kabashi E, Valdmanis PN, Dion P et al (2008) TARDBP mutations in individuals with sporadic and familial amyotrophic lateral sclerosis. Nat Genet 40:572–574
16. Kawahara Y, Ito K, Sun H et al (2004) Glutamate receptors: RNA editing and death of motor neurons. Nature 427:801
17. Kawahara Y, Ito K, Ito M, Tsuji S, Kwak S (2005) Novel splice variants of human ADAR2 mRNA: skipping of the exon encoding the dsRNA-binding domains, and multiple C-terminal splice sites. Gene 363:193–201
18. Kawahara Y, Kwak S (2005) Excitotoxicity and ALS: what is unique about the AMPA receptors expressed on spinal motor neurons? Amyotroph Lateral Scler Other Motor Neuron Disord 6:131–144
19. Kawahara Y, Sun H, Ito K et al (2006) Underediting of GluR2 mRNA, a neuronal death inducing molecular change in sporadic ALS, does not occur in motor neurons in ALS1 or SBMA. Neurosci Res 54:11–14
20. Kwak S, Kawahara Y (2005) Deficient RNA editing of GluR2 and neuronal death in amyotropic lateral sclerosis. J Mol Med 83:110–120
21. Kwak S, Weiss JH (2006) Calcium-permeable AMPA channels in neurodegenerative disease and ischemia. Curr Opin Neurobiol 16:281–287
22. Kwiatkowski TJ Jr, Bosco DA, Leclerc AL et al (2009) Mutations in the FUS/TLS gene on chromosome 16 cause familial amyotrophic lateral sclerosis. Science 323:1205–1208
23. Mackenzie IR, Bigio EH, Ince PG et al (2007) Pathological TDP-43 distinguishes sporadic amyotrophic lateral sclerosis from amyotrophic lateral sclerosis with SOD1 mutations. Ann Neurol 61:427–434
24. Nakashima-Yasuda H, Uryu K, Robinson J et al (2007) Comorbidity of TDP-43 proteinopathy in Lewy body related diseases. Acta Neuropathol 114:221–229
25. Neumann M, Sampathu DM, Kwong LK et al (2006) Ubiquitinated TDP-43 in frontotemporal lobar degeneration and amyotrophic lateral sclerosis. Science 314:130–133
26. Neumann M, Kwong LK, Lee EB et al (2009) Phosphorylation of S409/410 of TDP-43 is a consistent feature in all sporadic and familial forms of TDP-43 proteinopathies. Acta Neuropathol 117:137–149
27. Nishimura AL, Mitne-Neto M, Silva HC et al (2004) A mutation in the vesicle-trafficking protein VAPB causes late-onset spinal muscular atrophy and amyotrophic lateral sclerosis. Am J Hum Genet 75:822–831
28. Ou SH, Wu F, Harrich D et al (1995) Cloning and characterization of a novel cellular protein, TDP-43, that binds to human immunodeficiency virus type 1 TAR DNA sequence motifs. J Virol 69:3584–3596
29. Paschen W, Hedreen JC, Ross CA (1994) RNA editing of the glutamate receptor subunits GluR2 and GluR6 in human brain tissue. J Neurochem 63:1596–1602
30. Rosen DR, Siddique T, Patterson D et al (1993) Mutations in Cu/Zn superoxide dismutase gene are associated with familial amyotrophic lateral sclerosis. Nature 362:59–62
31. Sommer B, Köhler M, Sprengel R, Seeburg PH (1991) RNA editing in brain controls a determinant of ion flow in glutamate-gated channels. Cell 67:11–19
32. Sreedharan J, Blair IP, Tripathi VB et al (2008) TDP-43 mutations in familial and sporadic amyotrophic lateral sclerosis. Science 319:1668–1672
33. Suzuki T, Tsuzuki K, Kameyama K, Kwak S (2003) Recent advances in the study of AMPA receptors. Nippon Yakurigaku Zasshi 122:515–526
34. Takuma H, Kwak S, Yoshizawa T, Kanazawa I (1999) Reduction of GluR2 RNA editing, a molecular change that increases calcium influx through AMPA receptors, selective in the spinal

ventral gray of patients with amyotrophic lateral sclerosis. Ann Neurol 46:806–815
35. Tan CF, Eguchi H, Tagawa A et al (2007) TDP-43 immunoreactivity in neuronal inclusions in familial amyotrophic lateral sclerosis with or without SOD1 gene mutation. Acta Neuropathol 113:535–542
36. Uryu K, Nakashima-Yasuda H, Forman MS et al (2008) Concomitant TAR-DNA-binding protein 43 pathology is present in Alzheimer disease and corticobasal degeneration but not in other tauopathies. J Neuropathol Exp Neurol 67:555–564
37. Van Deerlin VM, Leverenz JB, Bekris LM et al (2008) TARDBP mutations in amyotrophic lateral sclerosis with TDP-43 neuropathology: a genetic and histopathological analysis. Lancet Neurol 7:409–416
38. Vance C, Rogelj B, Hortobágyi T et al (2009) Mutations in FUS, an RNA processing protein, cause familial amyotrophic lateral sclerosis type 6. Science 323:1208–1211
39. Yang Y, Hentati A, Deng HX et al (2001) The gene encoding alsin, a protein with three guanine-nucleotide exchange factor domains, is mutated in a form of recessive amyotrophic lateral sclerosis. Nat Genet 29:160–165
40. Yokoseki A, Shiga A, Tan CF et al (2008) TDP-43 mutation in familial amyotrophic lateral sclerosis. Ann Neurol 63:538–542

Supplementary Data

Materials and Methods

ADAR2 in degenerating neurons in other neurological diseases

Formalin-fixed paraffin-embedded sections at the level of the pontine nuclei were obtained from patients with ALS (case 4 in the Table), multiple system atrophy (73 y, female), or spinocerebellar atrophy type 1 (53 y, male) to examine the disease specificity of the alteration in ADAR2 expression in ALS spinal motor neurons. Immunohistochemistry was performed as described in the Materials and Methods section in the text.

Immunohistochemistry with several different anti-ADAR2 antibodies.

In addition to the RED1 antibody, another anti-ADAR2 antibodies, C-15 (Santa Cruz Biotechnology, Santa Cruz, CA), was used. The antibody was diluted (1:100) and incubated with the samples overnight at 4°C. The C-15 ADAR2 antibody recognizes the long C-terminus. This experiment was done using the spinal cord sections from a control subject (case 12 in the Table).

Supplementary Figure 1

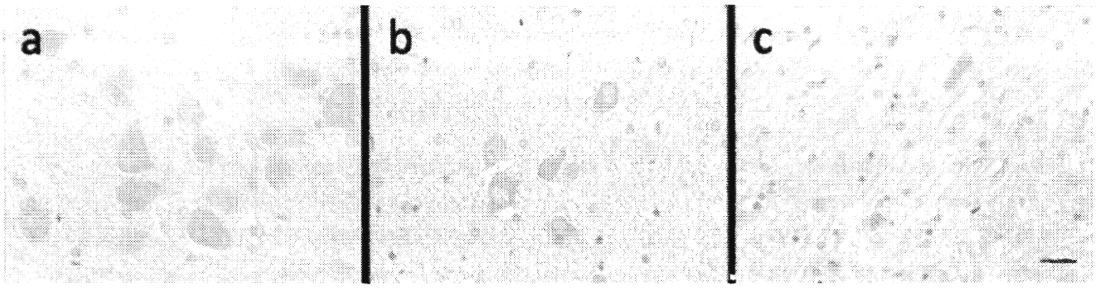

ADAR2 immunostaining in degenerating neurons in other neurological diseases. Neurons in the pontine nuclei of an ALS patient exhibit slight ADAR2 immunoreactivity in the cytoplasm (a). The neurons in the pontine nuclei in both multiple system atrophy (b) and spinocerebellar atrophy type 1 (c) showed faint ADAR2 immunoreactivity, although these neurons were atrophic and reduced in number. These results suggested that the alteration of ADAR2 activity was not involved in the process of neuronal death in the pontine nucleus of MSA or SCA1. Bar indicates 20 μm.

Supplementary Figure 2

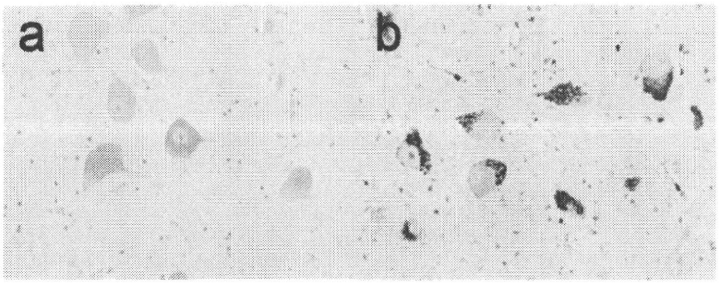

Immunohistochemistry with two anti-ADAR2 antibodies. Both RED1 (a) and C-15 (b) stained specifically the cytoplasm but not the nucleus of motor neurons. Non-specific lipofuscin staining is observed in (b).

nature neuroscience

Astrocytes as determinants of disease progression in inherited amyotrophic lateral sclerosis

Koji Yamanaka[1,2], Seung Joo Chun[1], Severine Boillee[1], Noriko Fujimori-Tonou[2], Hirofumi Yamashita[2], David H Gutmann[3], Ryosuke Takahashi[4], Hidemi Misawa[5] & Don W Cleveland[1]

Dominant mutations in superoxide dismutase cause amyotrophic lateral sclerosis (ALS), an adult-onset neurodegenerative disease that is characterized by the loss of motor neurons. Using mice carrying a deletable mutant gene, diminished mutant expression in astrocytes did not affect onset, but delayed microglial activation and sharply slowed later disease progression. These findings demonstrate that mutant astrocytes are viable targets for therapies for slowing the progression of non–cell autonomous killing of motor neurons in ALS.

ALS is an adult-onset neurodegenerative disease, characterized by a progressive and fatal loss of motor neurons. Dominant mutations in the gene for superoxide dismutase (*SOD1*) are the most frequent cause of inherited ALS. Ubiquitous expression of mutant *SOD1* in rodents leads to progressive, selective motor neuron degeneration as a result of acquired toxic properties. The exact mechanism responsible for motor neuron degeneration in ALS, however, is not known[1,2]. Mutant damage in the vulnerable motor neurons is a key determinant of disease onset[3], whereas accumulating evidence supports an active role of non-neuronal cells in motor neuron degeneration[3–7]. Evidence with selective gene excision[3] or bone-marrow grafting[5] has demonstrated that mutant SOD1-derived damage in microglia accelerates later disease progression. Despite the importance of astrocyte function, the role of mutant action in astrocytes in disease has not been tested *in vivo*.

To examine whether mutant SOD1 damage in astrocytes contributes to disease, *loxSOD1*^{G37R} mice[3], carrying a mutant *SOD1* gene that can be deleted by the action of the Cre recombinase, were mated with *GFAP-Cre* mice (**Fig. 1** and **Supplementary Fig. 1** online), which express both Cre recombinase and β-galactosidase (*LacZ*) under the control of the human GFAP promoter[8]. Mice from these matings that carry the *GFAP-Cre* transgene are denoted as Cre$^+$, whereas mice without it are referred to as Cre$^-$. To determine the cell-type specificity of Cre expression in the spinal cord, *GFAP-Cre* mice were mated to Rosa26 mice, which ubiquitously express a *LacZ* gene that encodes functional β-galactosidase only after Cre-mediated recombination. Although this *GFAP-Cre* transgene is expressed in a subset of neurons in the cerebellum and hippocampus during embryogenesis[9], measurement of β-galactosidase activity (by deposition of a blue reaction product after addition of the X-gal substrate) demonstrated that Cre expression and Cre-mediated recombination was restricted in the spinal cord to GFAP-reactive astrocytes (**Fig. 1a,b**). The efficiency of mutant gene excision in cultured astrocytes from newborn *loxSOD1*^{G37R}*/GFAP-Cre*$^+$ mice was ~76% (**Fig. 1d,e**), determined by quantitative PCR for human SOD1 transgene number (**Fig. 1d**) and immunoblotting for mutant SOD1 levels (**Fig. 1e**). We observed neither detectable Cre activity nor mutant gene excision in microglia (**Fig. 1c** and **Supplementary Fig. 2** online).

A simple, objective measure of disease onset and early disease was applied by initiation of weight loss, itself reflecting denervation-induced muscle atrophy. Reduction of SOD1^{G37R} in astrocytes did not slow disease onset nor early disease (GFAP-Cre$^+$, 341.6 ± 48.9 d; GFAP-Cre$^-$, 337.0 ± 35.8 d; **Fig. 1f,h**). However, late disease progression (from early disease to end stage) was sharply delayed, providing a mean extension of survival by 48 d (Cre$^+$, 87.4 d; Cre$^-$, 39.5 d; **Fig. 1j**). Progression from onset to early disease was more modestly slowed by 14 d (Cre$^+$, 99.3 d; Cre$^-$, 85.2 d; **Fig. 1i**). Overall survival was extended by 60 d (Cre$^+$, 436.5 ± 38.8 d; Cre$^-$, 376.5 ± 26.9 d; **Fig. 1g**). This contrasts with delayed disease onset from diminished mutant synthesis solely within motor neurons (with a *VAChT-Cre* transgene carrying the motor neuron–specific vesicular acetylcholine transporter promoter) without affecting disease progression (**Supplementary Results, Supplementary Methods** and **Supplementary Fig. 3** online), just as reported previously with an *Isl1* (*Islet1*)*-Cre* transgene that is expressed in motor neurons and some peripheral tissues[3].

Astrocytic and microglial cell activation is a well-accepted feature of SOD1 mutant–mediated ALS[1,2]. An elevated proportion of GFAP-positive astrocytes appeared before disease onset (**Fig. 2a**) in *loxSOD1*^{G37R} mice. This astrogliosis was progressive, readily apparent by onset (**Fig. 2b**) and more prominent during disease progression (**Fig. 2c**). Despite substantial mutant reduction, astrogliosis was not, however, different in comparing disease-matched *loxSOD1*^{G37R}*/GFAP-Cre*$^+$ mice (**Fig. 2d,e**) and *loxSOD1*^{G37R}*/GFAP-Cre*$^-$ mice (**Fig. 2b,c**).

Microglial activation occurred at earliest disease onset in *Cre*$^-$ mice (**Fig. 2g**) and was progressively more prominent during disease progression (**Fig. 2h**). Microglial activation was, however, substantially delayed from onset through early disease in the *GFAP-Cre*$^+$ mice when mutant SOD1 levels were reduced only in astrocytes (**Fig. 2i,j**). By exploiting the presence of β-galactosidase to mark astrocytes with diminished SOD1 mutant synthesis, examination of sections throughout lumbar spinal cords of symptomatic *loxSOD1*^{G37R}*/GFAP-Cre*$^+$ mice

[1]Ludwig Institute for Cancer Research and Department of Medicine and Neuroscience, University of California at San Diego, 9500 Gilman Drive, La Jolla, California 92093-0670, USA. [2]Yamanaka Research Unit, RIKEN Brain Science Institute, 2-1 Hirosawa, Wako, Saitama 351-0198, Japan. [3]Department of Neurology, Washington University School of Medicine, 660 South Euclid Avenue, St. Louis, Missouri 63110, USA. [4]Department of Neurology, Graduate School of Medicine, Kyoto University, 54 Shogoin Kawahara-cho, Sakyo-ku, Kyoto 606-8507, Japan. [5]Department of Pharmacology, Kyoritsu University of Pharmacy, 1-5-30 Shibakoen, Minato-ku, Tokyo 105-8512, Japan. Correspondence should be addressed to D.W.C. (dcleveland@ucsd.edu) or K.Y. (kyamanaka@brain.riken.jp).

Received 26 November 2007; accepted 7 January 2008; published online 3 February 2008; doi:10.1038/nn2047

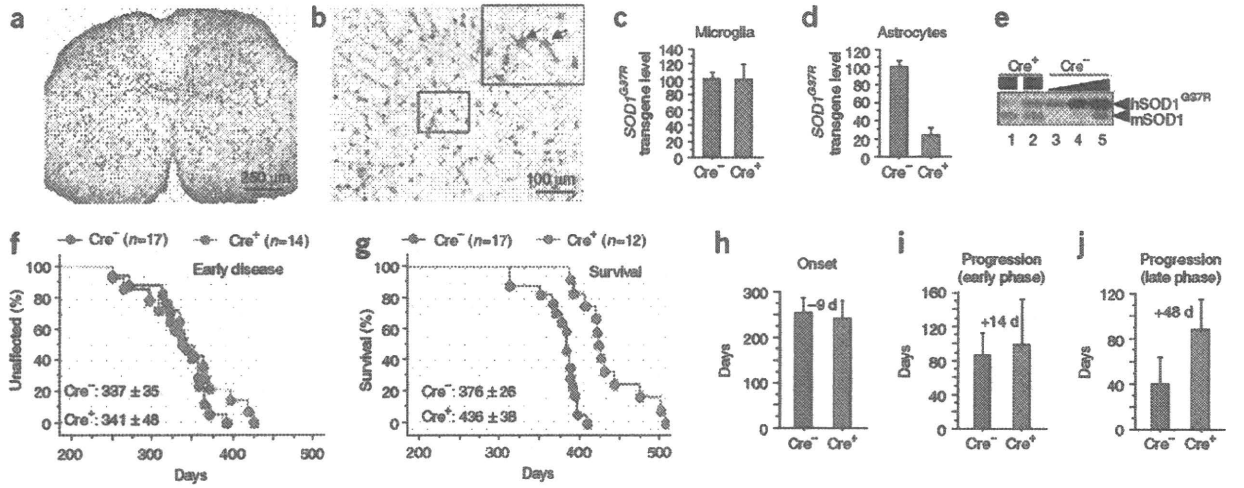

Figure 1 Selective Cre-mediated gene excision shows that mutant SOD1 action in astrocytes is a primary determinant of late disease progression. (**a**,**b**) β-galactosidase (β-gal) activity in astrocytes in whole (**a**) or in the anterior horn region (**b**) of the lumbar spinal cord section of *GFAP-Cre*/Rosa26 reporter mice visualized with X-gal and immunostaining with GFAP antibody. Inset, magnified image of the boxed area in **b**. Arrows indicate β-gal/GFAP-Cre–expressing astrocytes. (**c**,**d**) *loxSOD1*^{G37R} transgene levels ($n = 3$ for each group) in primary microglia (**c**) or astrocytes (**d**) from *loxSOD1*^{G37R}/*GFAP-Cre*$^{+}$ and *loxSOD1*^{G37R} mice using real-time PCR. (**e**) We determined SOD1^{G37R} and mouse SOD1 levels by immunoblotting extracts from isolated primary astrocytes of *loxSOD1*^{G37R}/*GFAP-Cre*$^{+}$ (lanes 1, 2) and a dilution series of a comparable extract from LoxSOD1^{G37R} astrocytes representing 25%, 50% and 100% of the protein amounts loaded in lanes 1 and 2 (lanes 3–5). (**f**,**g**) Ages at which early disease phase (to 10% weight loss, $P = 0.76$; **f**) or end-stage disease ($P < 0.0001$; **g**) were reached for *loxSOD1*^{G37R}/*GFAP-Cre*$^{+}$ mice (red) and *loxSOD1*^{G37R} littermates (blue). Mean ages ± s.d. are provided. (**h**–**j**) Mean onset ($P = 0.47$) (**h**), mean duration of early disease (from onset to 10% weight loss, $P = 0.35$; **i**) and a late disease (from 10% weight loss to end stage, $P < 0.0001$; **j**) for *loxSOD1*^{G37R}/*GFAP-Cre*$^{+}$ (red) and *loxSOD1*^{G37R} littermates (blue). At each time point, *P* value was determined by unpaired *t*-test. Error bars denote s.d.

revealed an inverse relationship (**Fig. 3a–g**) between the number of astrocytes with reduced mutant SOD1 (*Cre*$^{+}$) and activated microglia (correlation coefficient, $r = -0.868$, $P < 0.001$), despite comparable astrocytic activation. Thus, microglial activation was most prominent in areas with the highest mutant SOD1–expressing astrocyte concentration.

Elevated production of nitric oxide by upregulated inducible nitric oxide synthase (iNOS) has been reported in mutant SOD1 mice[10], although deletion of the iNOS gene has modest[11] or no[12] effect on SOD1-mediated disease. It is not known in which glial cells this nitric oxide is produced in *in vivo* models of ALS, although both microglia and astrocytes have an ability to produce it when stimulated *in vitro*[13]. Triple staining of lumbar spinal cord sections with iNOS, Mac2 and GFAP antibodies (**Fig. 3h–r**) revealed that almost all iNOS-positive cells were Mac2-positive microglia (**Fig. 3n–r** and **Supplementary Fig. 4** online), indicating that activated microglia are the primary cell type producing nitric oxide in this SOD1 mouse model. Diminishing mutant synthesis in astrocytes inhibited iNOS induction in disease-matched, symptomatic SOD1 mice (**Fig. 3h,k**), consistent with substantial inhibition of microglial activation (**Fig. 3i,l**).

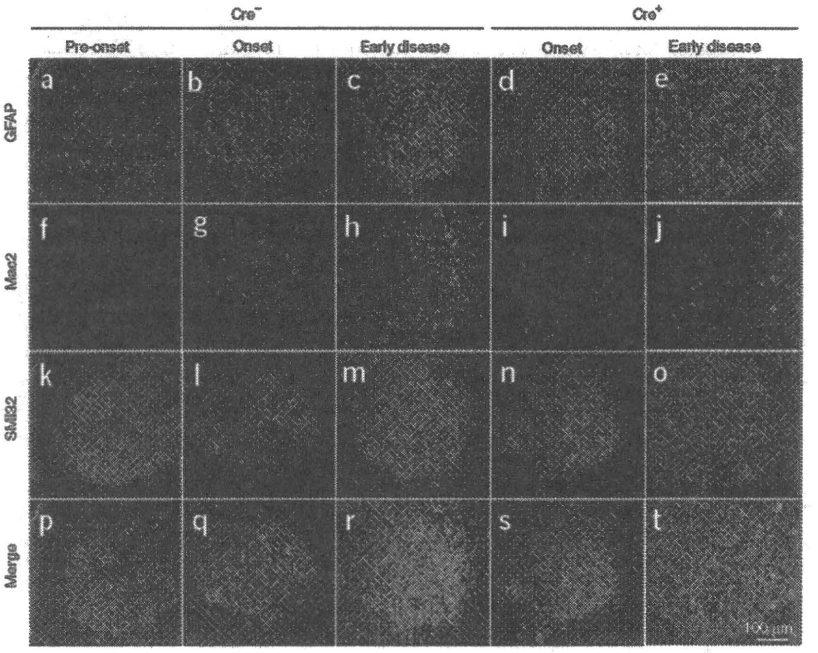

Figure 2 Selective downregulation of mutant SOD1 in astrocytes significantly inhibits microglial activation. (**a**–**t**) GFAP-positive astrocytes (**a**–**e**), Mac2-positive activated microglia (**f**–**j**) and motor neurons identified with the neurofilament antibody SMI-32 (**k**–**o**) in the lumbar spinal cord of a *loxSOD1*^{G37R} mouse before disease onset (**a**,**f**,**k**,**p**), at disease onset (**b**,**g**,**l**,**q**) or during early disease (**c**,**h**,**m**,**r**), together with *loxSOD1*^{G37R}/*GFAP-Cre*$^{+}$ mice at disease onset (**d**,**i**,**n**,**s**) or during early disease (**e**,**j**,**o**,**t**). Merged images are shown in **p**–**t**.

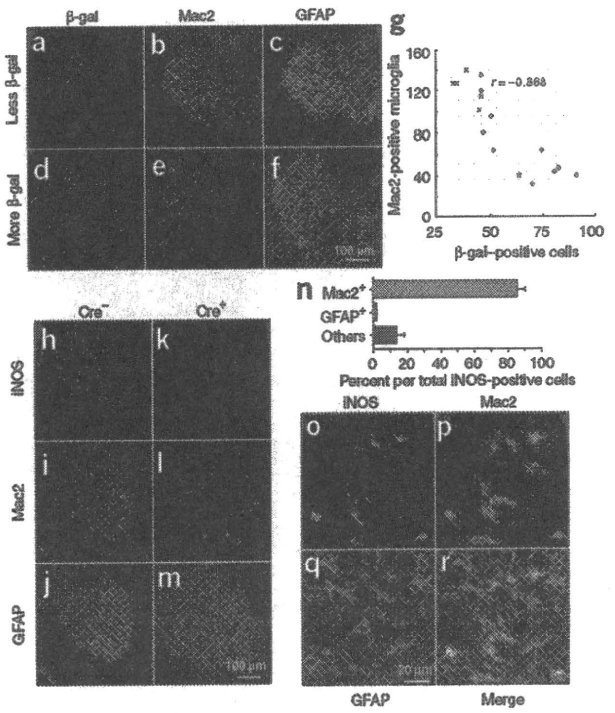

Figure 3 Mutant-expressing astrocytes enhance microglial activation and induction of iNOS. (**a–f**) Images of β-galactosidase (**a**,**d**), Mac2 (**b**,**e**) and GFAP (**c**,**f**) staining from a left (**a–c**) and right (**d–f**) lumbar spinal cord section from a 12-month-old *loxSOD1*^{G37R}*/GFAP-Cre*$^{+}$ mouse. *GFAP-Cre*$^{+}$ astrocytes are marked by β-galactosidase (**a**,**d**). (**g**) Inverted correlation between the number of Cre-positive astrocytes and Mac2-positive microglia in *loxSOD1*^{G37R}*/GFAP-Cre*$^{+}$ mice lumbar spinal cord sections (correlation coefficient, $r = -0.868$, $P < 0.001$). (**h–m**) Lumbar spinal cord sections from *loxSOD1*^{G37R} (**h–j**) and *loxSOD1*^{G37R}*/GFAP-Cre*$^{+}$ (**k–m**) mice at the early disease stage immunostained with antibodies to iNOS (**h**,**k**), Mac2 (**i**,**l**), and GFAP (**j**,**m**). (**n**) Quantification of iNOS-positive cells in the anterior horn from lumbar spinal cord of symptomatic *loxSOD1*^{G37R} mice. We plotted the averaged percent of iNOS^{+}/Mac2^{+} (red), iNOS^{+}/GFAP^{+} (blue) and iNOS^{+}/other cell type (black) per total iNOS^{+} cells. (**o–r**) Magnified images of anterior horn from lumbar spinal cord of symptomatic *loxSOD1*^{G37R} mice stained with iNOS (**o**), Mac2 (**p**) and GFAP (**q**). Merged image illustrates that iNOS-positive cells are Mac2-positive microglia (**r**).

A role for astrocytes in inherited ALS has been previously considered in several contexts. Mutant-expressing astrocytes produce and release one or more as yet uncharacterized components that can accelerate motor neuron death *in vitro*[6,7]. Focal loss of the astrocytic EAAT2 glutamate transporter in affected regions[14] (**Supplementary Fig. 5** online) and the failure of normal glutamate uptake of *SOD1*^{G93A} astrocytes *in vitro*[15] support glutamate-dependent excitotoxicity as a component of disease. Nevertheless, diminished mutant SOD1 synthesis in most astrocytes did not affect disease-dependent loss of EAAT2 from those astrocytes (**Supplementary Fig. 5**), indicating that a reduction in glutamate transport reflects non–cell autonomous damage to astrocytes, in part, from mutant SOD1 synthesized by other cells. Our use of selective gene excision has now demonstrated that mutant SOD1 damage in both microglia[3] and astrocytes (**Fig. 1g–j**) accelerates later disease progression without affecting the initiation of motor neuron degeneration and phenotypic disease onset. Discovery that damage in astrocytes determines the timing of microglial activation and infiltration provides further evidence that, beyond any direct effect of mutant astrocytes on motor neurons, such astrocytes amplify an inflammatory response from microglia (including enhanced production of nitric oxide and possibly of toxic cytokines), leading to further damage to the motor neurons and accelerated disease progression through a non–cell autonomous mechanism (**Supplementary Fig. 6** online). These findings validate therapies, including astrocytic stem cell–replacement approaches, that aim to slow disease progression in ALS by supplementing healthy astrocytes or modulating toxicity in astrocytes to control an inflammatory response of microglia.

Note: Supplementary information is available on the Nature Neuroscience website.

ACKNOWLEDGMENTS

This work was supported by a US National Institutes of Health grant (NS 27036) and a grant from the Packard ALS Center at Johns Hopkins (D.W.C.), as well as a Muscular Dystrophy Association developmental grant, the Uehara Memorial Foundation, the Nakabayashi Trust for ALS Research and a grant-in-aid for Scientific Research (19591021) and on Priority Area (19044048) from the Ministry of Education, Culture, Sports, Science and Technology of Japan (K.Y.). Salary support for D.W.C is provided by the Ludwig Institute for Cancer Research. S.B. is a recipient of a Fondation pour la Recherche Medical fellowship, an Institut National de la santé et de la Recherché Medicale fellowship and a Muscular Dystrophy Association developmental grant.

AUTHOR CONTRIBUTIONS

K.Y., S.J.C., S.B., N.F.-T. and H.Y. conducted the experiments. D.H.G., R.T. and H.M. provided essential experimental tools and advice. K.Y., S.B., and D.W.C. were responsible for the overall design of the project, analyses of the results and writing the manuscript.

Published online at http://www.nature.com/natureneuroscience
Reprints and permissions information is available online at http://npg.nature.com/reprintsandpermissions

1. Pasinelli, P. & Brown, R.H. *Nat. Rev. Neurosci.* **7**, 710–723 (2006).
2. Boillee, S., Vande Velde, C. & Cleveland, D.W. *Neuron* **52**, 39–59 (2006).
3. Boillee, S. *et al. Science* **312**, 1389–1392 (2006).
4. Clement, A.M. *et al. Science* **302**, 113–117 (2003).
5. Beers, D.R. *et al. Proc. Natl. Acad. Sci. USA* **103**, 16021–16026 (2006).
6. Di Giorgio, F.P., Carrasco, M.A., Siao, M.C., Maniatis, T. & Eggan, K. *Nat. Neurosci.* **10**, 608–614 (2007).
7. Nagai, M. *et al. Nat. Neurosci.* **10**, 615–622 (2007).
8. Bajenaru, M.L. *et al. Mol. Cell. Biol.* **22**, 5100–5113 (2002).
9. Fraser, M.M. *et al. Cancer Res.* **64**, 7773–7779 (2004).
10. Almer, G., Vukosavic, S., Romero, N. & Przedborski, S. *J. Neurochem.* **72**, 2415–2425 (1999).
11. Martin, L.J. *et al. J. Comp. Neurol.* **500**, 20–46 (2007).
12. Son, M., Fathallah-Shaykh, H.M. & Elliott, J.L. *Ann. Neurol.* **50**, 273 (2001).
13. Barbeito, L.H. *et al. Brain Res. Brain Res. Rev.* **47**, 263–274 (2004).
14. Howland, D.S. *et al. Proc. Natl. Acad. Sci. USA* **99**, 1604–1609 (2002).
15. Vermeiren, C. *et al. J. Neurochem.* **96**, 719–731 (2006).

Experimental Neurology 217 (2009) 235–236

Contents lists available at ScienceDirect

Experimental Neurology

journal homepage: www.elsevier.com/locate/yexnr

Commentary

Edaravone in ALS

Ryosuke Takahashi

Department of Neurology, Kyoto University Graduate School of Medicine, 54 Shogoin-Kawaharacho, Sakyoku, Kyoto 606-8507, Japan

ARTICLE INFO

Article history:
Received 30 December 2008
Revised 28 February 2009
Accepted 3 March 2009
Available online 10 March 2009

Amyotrophic lateral sclerosis (ALS) is a devastating neurodegenerative disorder characterized by progressive and relatively selective degeneration of upper and lower motor neurons. Patients suffer from atrophy and paralysis of systemic voluntary muscles including respiratory muscles, leading to respiratory failure and subsequent death 3–5 years after the disease onset. Effective therapy for ALS that ameliorates its clinical course is still not known (Mitchell and Borasio, 2007).

Although ALS usually develops sporadically, 5 to 10% of cases are familial and hereditary. Twenty percent of familial ALS (FALS) are caused by mutations in the *copper and zinc-dependent superoxide dismutase* (*SOD1*) gene, which was first reported in 1993 (Rosen et al., 1993). Mutant SOD1 brought a breakthrough to this field, since mutant SOD1 transgenic mice recapitulate the clinical symptoms and pathological findings of human FALS (Gurney et al., 1994). Mutant SOD1 transgenic mouse models provided invaluable tools for testing effective drugs which extend their lifespan. Up to now, more than 20 drugs have been claimed to be effective in the therapy of mouse ALS.

A big problem, however, is arising: none of these drugs have yet to be shown to be effective as well in human sporadic ALS (SALS) patients (Benatar, 2007). Why? A couple of explanations are conceivable. First, mutant SOD1 transgenic mice may not be a good model for human sporadic ALS cases despite their apparent similarities. Indeed, mutant SOD1 associated FALS and SALS exhibit different microscopic neuropathology. The former is characterized by Lewy body-like inclusion containing mutant SOD1, whereas for the latter skein-like or round inclusions containing TDP-43. Since TDP-43 is implicated in the pathogenesis of SALS as well as in a subgroup of FALS, developing a new ALS mouse model based on TDP-43 could solve these problems in the future (Neumann et al., 2007). A second possible explanation is that the most therapies in mouse models are initiated prior to disease onset, which is impossible in human patients until presymptomatic diagnosis for ALS becomes available. Thirdly, whether drug dosage and bioavailablity comparable to mouse experiments are replicated in human trials remains unclear.

An alternative explanation is the difference in the design of mouse experimental therapies and human clinical trials. Randomized controlled trials, which are designed to eliminate numerous confounding factors including observation biases, are standard in human clinical trials. In contrast, mouse experiments are generally not performed as rigorously as human trials, increasing risks of producing "false positive" results (Benatar, 2007).

Edaravone (3-methyl-1-phenyl-2-pyrazolin-5-one) is a free radical scavenger that has been approved in Japan since 2001 as a therapeutic agent to reduce neuronal damage caused by acute ischemic stroke (Yoshida et al., 2006). Edaravone eliminates lipid peroxide and hydroxyl radicals by transferring an electron to the radical, thereby ameliorating the ischemic neuronal damage. Oxidative stress is implicated as one of the pathogenetic mechanisms for ALS (Barber et al., 2006). Moreover, a small-sized open trial of edaravone suggested that edaravone is safe and may delay the progression of functional motor disturbances in ALS patients (Yoshino and Kimura, 2006). Thus. edaravone is a promising therapeutic agent for human motor neuron diseases including ALS.

In a previous issue, Ito et al. reported an experimental therapy of a mutant SOD1 mouse model using edaravone (Ito et al., 2008). Taking the problems associated with the therapeutic experimental design in mouse experiments, they carefully optimized the dosage of edaravone so that the pharmacokinetic profile after intraperitoneal injection became comparable to that in human patients. Moreover, they started treatment only after the disease onset, similar to human ALS treatment. Furthermore, they used only female mice for analysis considering the gender difference in lifespan and randomized blind analyses were adopted for all the behavioral as well as pathological observations. This methodological rigorousness has never been considered seriously in previous experimental therapies of mutant SOD1 ALS mouse models, most of which have failed to be replicated in human patients.

Edaravone significantly slowed the motor function decline as assessed by multiple behavioral tests such as rotarod tests. However, the lifespan of edaravone-treated mice were not significantly higher

Fax: +81 75 761 9780.
E-mail address: ryosuket@kuhp.kyoto-u.ac.jp.

0014-4886/$ – see front matter
doi:10.1016/j.expneurol.2009.03.001

than those of control mice, suggesting that edaravone may improve the motor function of the ALS mice without apparent lifespan expanding effects (Ito et al., 2008). This uncoupling in the mechanisms underlying motor function and lifespan further implies that pathways causing motor function decline are not necessarily the ones causing eventual death, usually by respiratory muscle failure. That said, it would be possible to identify drugs that can improve the quality of life in ALS patients without affecting lifespan, which seems to be an easier goal compared with identifying lifespan-extending drugs for ALS. Moreover, it was clinically important that edaravone was effective even when administered after the disease onset. On the other hand, it would be intriguing to administer edaravone to ALS mice at their presymptomatic stage to understand how the point at which edaravone is used during the course of disease affects its outcome.

It is noted that high-dose edaravone treatment leads to a decrease of mutant SOD1 accumulation in the spinal cord. Since administration of edaravone resulted in a marked decrease of 3-nitrotyrosine/tyrosine ratio, a marker of oxidative stress, suppression of oxidative stress is likely to be upstream of the inhibition of aggregate formation (Kabashi and Durham, 2006; Valentine and Hart, 2003). It has long been debated how oxidative stress is induced by SOD1 mutations (Barber et al., 2006). Reduced enzymatic activity of SOD1 and generation of peroxynitrite due to aberrant copper chemistry have been proposed as plausible mechanism explaining "gain of toxic function" of mutant SOD1 (Beckman et al., 1993; Deng et al., 1993; Robberecht et al., 1994). However, the fact that a subgroup of SOD1 mutants retains full enzymatic activity and that H46R and H48Q mutants which completely lose binding sites for copper still cause ALS suggests that mechanisms unrelated to SOD1 activity may also be involved (Borchelt et al., 1994; Valentine et al., 2005; Wang et al., 2003). It has been shown that mutant SOD1 overexpression in a neuronal cell line leads to transcriptional repression of antioxidant proteins by reducing the level of transcriptional factor NRF2 (Kirby et al., 2005). It would be intriguing to investigate whether edaravone affects the level of NRF2 when administered to ALS mice.

Another interesting unresolved question is which cells are the targets of edaravone. Recently, it has been shown that motor neuron death in mutant SOD1 ALS mouse models is non-cell autonomous (Boillee et al., 2006; Yamanaka et al., 2008). In other words, mutant SOD1-expressing astroglial or miroglial cells promote motor neuron death. In this context, edarovone may decrease the aggregates in non-neuronal glial cells, resulting in amelioration of neurodegeneration. These questions should be addressed in further analysis in the future.

A recent systematic review of randomized controlled trials of antioxidant therapies against ALS including vitamin E and acetylcysteine has shown that there is no substantial evidence to support their clinical use (Orrell et al., 2008). However, the evidence for the bene cial effects of edaravone on human ALS patients awaits the publication of the results of a phase III clinical trial of ALS, currently ongoing in Japan (http://www.als.net/research/studies/tdfAnimalStudyList.asp).

Acknowledgment

I thank Roberto Gavinio for kindly editing this manuscript.

References

Barber, S.C., Mead, R.J., Shaw, P.J., 2006. Oxidative stress in ALS: a mechanism of neurodegeneration and a therapeutic target. Biochim. Biophys. Acta 1762, 1051–1067.

Beckman, J.S., Carson, M., Smith, C.D., Koppenol, W.H., 1993. ALS, SOD and peroxynitrite. Nature 364, 584.

Benatar, M., 2007. Lost in translation: treatment trials in the SOD1 mouse and in human ALS. Neurobiol. Dis. 26, 1–13.

Boillee, S., Yamanaka, K., Lobsiger, C.S., Copeland, N.G., Jenkins, N.A., Kassiotis, G., Kollias, G., Cleveland, D.W., 2006. Onset and progression in inherited ALS determined by motor neurons and microglia. Science 312, 1389–1392.

Borchelt, D.R., Lee, M.K., Slunt, H.S., Guarnieri, M., Xu, Z.S., Wong, P.C., Brown Jr., R.H., Price, D.L., Sisodia, S.S., Cleveland, D.W., 1994. Superoxide dismutase 1 with mutations linked to familial amyotrophic lateral sclerosis possesses signi cant activity. Proc. Natl. Acad. Sci. U. S. A. 91, 8292–8296.

Deng, H.X., Hentati, A., Tainer, J.A., Iqbal, Z., Cayabyab, A., Hung, W.Y., Getzoff, E.D., Hu, P., Herzfeldt, B., Roos, R.P., et al., 1993. Amyotrophic lateral sclerosis and structural defects in Cu,Zn superoxide dismutase. Science 261, 1047–1051.

Gurney, M.E., Pu, H., Chiu, A.Y., Dal Canto, M.C., Polchow, C.Y., Alexander, D.D., Caliendo, J., Hentati, A., Kwon, Y.W., Deng, H.X., et al., 1994. Motor neuron degeneration in mice that express a human Cu,Zn superoxide dismutase mutation. Science 264, 1772–1775.

Ito, H., Wate, R., Zhang, J., Ohnishi, S., Kaneko, S., Ito, H., Nakano, S., Kusaka, H., 2008. Treatment with edaravone, initiated at symptom onset, slows motor decline and decreases SOD1 deposition in ALS mice. Exp. Neurol. 213, 448–455.

Kabashi, E., Durham, H.D., 2006. Failure of protein quality control in amyotrophic lateral sclerosis. Biochim. Biophys. Acta 1762, 1038–1050.

Kirby, J., Halligan, E., Baptista, M.J., Allen, S., Heath, P.R., Holden, H., Barber, S.C., Loynes, C.A., Wood-Allum, C.A., Lunec, J., Shaw, P.J., 2005. Mutant SOD1 alters the motor neuronal transcriptome: implications for familial ALS. Brain 128, 1686–1706.

Mitchell, J.D., Borasio, G.D., 2007. Amyotrophic lateral sclerosis. Lancet 369, 2031–2041.

Neumann, M., Kwong, L.K., Sampathu, D.M., Trojanowski, J.Q., Lee, V.M., 2007. TDP-43 proteinopathy in frontotemporal lobar degeneration and amyotrophic lateral sclerosis: protein misfolding diseases without amyloidosis. Arch. Neurol. 64, 1388–1394.

Orrell, R.W., Lane, R.J., Ross, M., 2008. A systematic review of antioxidant treatment for amyotrophic lateral sclerosis/motor neuron disease. Amyotroph. Lateral Scler. 9, 195–211.

Robberecht, W., Sapp, P., Viaene, M.K., Rosen, D., McKenna-Yasek, D., Haines, J., Horvitz, R., Theys, P., Brown Jr., R., 1994. Cu/Zn superoxide dismutase activity in familial and sporadic amyotrophic lateral sclerosis. J. Neurochem. 62, 384–387.

Rosen, D.R., Siddique, T., Patterson, D., Figlewicz, D.A., Sapp, P., Hentati, A., Donaldson, D., Goto, J., O'Regan, J.P., Deng, H.X., et al., 1993. Mutations in Cu/Zn superoxide dismutase gene are associated with familial amyotrophic lateral sclerosis. Nature 362, 59–62.

Valentine, J.S., Hart, P.J., 2003. Misfolded CuZnSOD and amyotrophic lateral sclerosis. Proc. Natl. Acad. Sci. U. S. A. 100, 3617–3622.

Valentine, J.S., Doucette, P.A., Zittin Potter, S., 2005. Copper-zinc superoxide dismutase and amyotrophic lateral sclerosis. Annu. Rev. Biochem. 74, 563–593.

Wang, J., Slunt, H., Gonzales, V., Fromholt, D., Coon eld, M., Copeland, N.G., Jenkins, N.A., Borchelt, D.R., 2003. Copper-binding-site-null SOD1 causes ALS in transgenic mice: aggregates of non-native SOD1 delineate a common feature. Hum. Mol. Genet. 12, 2753–2764.

Yamanaka, K., Chun, S.J., Boillee, S., Fujimori-Tonou, N., Yamashita, H., Gutmann, D.H., Takahashi, R., Misawa, H., Cleveland, D.W., 2008. Astrocytes as determinants of disease progression in inherited amyotrophic lateral sclerosis. Nat. Neurosci. 11, 251–253.

Yoshida, H., Yanai, H., Namiki, Y., Fukatsu-Sasaki, K., Furutani, N., Tada, N., 2006. Neuroprotective effects of edaravone: a novel free radical scavenger in cerebrovascular injury. CNS Drug Rev. 12, 9–20.

Yoshino, H., Kimura, A., 2006. Investigation of the therapeutic effects of edaravone, a free radical scavenger, on amyotrophic lateral sclerosis (Phase II study). Amyotroph. Lateral. Scler. 7, 241–245.

Neurobiology of Disease

Induced Loss of ADAR2 Engenders Slow Death of Motor Neurons from Q/R Site-Unedited GluR2

Takuto Hideyama,[1,2] Takenari Yamashita,[1,2] Takeshi Suzuki,[3] Shoji Tsuji,[2] Miyoko Higuchi,[5] Peter H. Seeburg,[5] Ryosuke Takahashi,[6] Hidemi Misawa,[4] and Shin Kwak[1,2]

[1]Core Research for Evolutional Science and Technology, Japan Science and Technology Agency and [2]Department of Neurology, Graduate School of Medicine, University of Tokyo, Bunkyo-ku, Tokyo 113-8655, Japan, [3]Division of Basic Biological Sciences and [4]Department of Pharmacology, Faculty of Pharmacy, Keio University, Minato-ku, Tokyo 105-8512, Japan, [5]Department of Molecular Neuroscience, Max Planck Institute of Medical Research, 69120 Heidelberg, Germany, and [6]Department of Neurology, Graduate School of Medicine, University of Kyoto, Sakyo-ku, Kyoto 606-8507, Japan

GluR2 is a subunit of the AMPA receptor, and the adenosine for the Q/R site of its pre-mRNA is converted to inosine (A-to-I conversion) by the enzyme called adenosine deaminase acting on RNA 2 (ADAR2). Failure of A-to-I conversion at this site affects multiple AMPA receptor properties, including the Ca^{2+} permeability of the receptor-coupled ion channel, thereby inducing fatal epilepsy in mice (Brusa et al., 1995; Feldmeyer et al., 1999). In addition, inefficient GluR2 Q/R site editing is a disease-specific molecular dysfunction found in the motor neurons of sporadic amyotrophic lateral sclerosis (ALS) patients (Kawahara et al., 2004). Here, we generated genetically modified mice (designated as AR2) in which the ADAR2 gene was conditionally targeted in motor neurons using the Cre/loxP system. These AR2 mice showed a decline in motor function commensurate with the slow death of ADAR2-deficient motor neurons in the spinal cord and cranial motor nerve nuclei. Notably, neurons in nuclei of oculomotor nerves, which often escape degeneration in ALS, were not decreased in number despite a significant decrease in GluR2 Q/R site editing. All cellular and phenotypic changes in AR2 mice were prevented when the mice carried endogenous GluR2 alleles engineered to express edited GluR2 without ADAR2 activity (Higuchi et al., 2000). Thus, loss of ADAR2 activity causes AMPA receptor-mediated death of motor neurons.

Introduction

GluR2 (also known as GluR-B or GluA2) is a subunit of the AMPA receptor. The adenosine within the glutamine codon for the Q/R site of its pre-mRNA is converted to inosine (A-to-I conversion) (Yang et al., 1995) by adenosine deaminase acting on RNA 2 (ADAR2) (Melcher et al., 1996). Because inosine is read as guanosine during translation, the genomic glutamine codon (Q: CAG) is converted to a codon for arginine (R: CIG) at the Q/R site of GluR2 in virtually all neurons in the mammalian brain (Seeburg, 2002). Conversion of Q to R at the Q/R site of GluR2 affects multiple AMPA receptor properties, including the Ca^{2+} permeability of the receptor-coupled ion channel, receptor trafficking, and assembly of receptor subunits (Sommer et al., 1991; Burnashev et al., 1992; Greger et al., 2002, 2003). Genetically modified mice in which the Q/R site of GluR2 remains unedited displayed fatal status epilepticus at early postnatal stages with exaggerated excitation of neurons (Brusa et al., 1995; Feldmeyer et al., 1999). Systemic ADAR2-null mice exhibit a similar phenotype, which was attributed to the absence of GluR2 Q/R site RNA editing (Higuchi et al., 2000). These findings indicate that the A-to-I conversion of the GluR2 Q/R site by ADAR2 is crucial for survival in mice. However, it has not been demonstrated whether neuronal death occurs in mice lacking GluR2 Q/R site editing or in those lacking ADAR2.

Amyotrophic lateral sclerosis (ALS) is the most common adult-onset motor neuron disease. Patients with sporadic ALS account for >90% of all cases, and the majority of them do not carry mutations in the causative genes of familial ALS that have been identified thus far (Schymick et al., 2007; Beleza-Meireles and Al-Chalabi, 2009). There is strong evidence indicating that AMPA receptor-mediated excitotoxic mechanism plays a pathogenic role in ALS and SOD1-associated familial ALS model animals (Rothstein et al., 1992; Carriedo et al., 1996; Van Damme et al., 2005). Recently, we demonstrated that a significant proportion of GluR2 mRNA was unedited at the Q/R site in spinal motor neurons of postmortem patients with sporadic ALS. This is in marked contrast to the fact that all GluR2 mRNA was edited in the motor neurons of control subjects (Takuma et al., 1999; Kawahara et al., 2004) and of patients with motor neuron diseases other than sporadic ALS (Kawahara et al., 2006), as well as in dying neurons in other neurodegenerative diseases, including Purkinje cells of patients with spinocerebellar degeneration (Paschen et al., 1994; Akbarian et al., 1995; Kawahara et al., 2004; Suzuki et al., 2003). The disease specificity of inefficient GluR2 Q/R site editing implies the pathogenic relevance of ADAR2 insufficiency in the death of motor neurons in sporadic ALS but

Received April 20, 2010; revised July 2, 2010; accepted July 13, 2010.

This study was supported in part by Ministry of Education, Culture, Sports, Science, and Technology of Japan Grants-in-Aid for Scientific Research 17390251, 19390235, and 20023008 (S.K.), Ministry of Health, Labor, and Welfare of Japan Grant H18-Kokoro-017 (S.K.), and Amyotrophic Lateral Sclerosis Association Grant 875 (P.H.S.). We thank Dr. R. B. Emeson at Vanderbilt University (Nashville, TN) for antibodies to ADAR2 and D. Kimura, K. Awabayashi, Dr. J. Shimizu, Dr. M. Fukaya, and T. Kakinoki for technical assistance.

Correspondence should be addressed to Dr. Shin Kwak, Department of Neurology, Graduate School of Medicine, University of Tokyo, 7-3-1 Hongo, Bunkyo-ku, Tokyo 113-8655, Japan. E-mail: kwak-tky@umin.ac.jp.

DOI:10.1523/JNEUROSCI.2021-10.2010

 0270-6474/10/3011917-09$15.00/0

leaves open the possibility that other genes whose products remain unedited by ADAR2 insufficiency might contribute to the demise of motor neurons.

We therefore generated a conditional ADAR2 knock-out mouse strain (designated here as AR2), using the Cre/loxP recombination system, and demonstrated that the loss of ADAR2 activity induces the slow death of motor neurons also in the mouse. Importantly, all motor neuron death in AR2 mice could be prevented by substituting the wild-type GluR2 alleles for alleles point mutated to express Q/R site-edited GluR2 in the absence of ADAR2. Our genetic studies in the mouse clearly demonstrate that the underediting of the GluR2 Q/R site specifically induces death of motor neurons with reduced ADAR2 activity.

Materials and Methods

All studies were performed in accordance with the Declaration of Helsinki, the Guideline of Animal Studies of the University of Tokyo, and National Institutes of Health. The committee of animal handling of the University of Tokyo also approved the experimental procedures used.

ADAR2^{flox} *allele and conditional ADAR2 knock-out mice.* DNA for the targeted region was obtained from a mouse strain 129/SvEv genomic library (supplemental Table S1, available at www.jneurosci.org as supplemental material). A LoxP site was inserted into intron 6 and another LoxP site was inserted into intron 9 of the mouse *ADAR2* gene (*adarb1*), along with a selection cassette containing a neomycin resistance gene (Neo) flanked by flippase recognition target (FRT) sites (Fig. 1*A*). Exons 7–9 encode the majority of the adenosine deaminase motif. Chimeric mice were generated by injection of a targeted embryonic stem cell clone into C57BL/6-derived blastocysts. *ADAR2*$^{flox/+}$ intercrosses produced *ADAR2*$^{flox/flox}$ mice at apparent Mendelian frequencies, and *ADAR2*$^{flox/flox}$ homozygous mice were phenotypically normal. Determination of the *ADAR2*^{flox} allele was conducted by genomic PCR (Fig. 1*B*). Then, to knock-out ADAR2 activity selectively in motor neurons, we crossed *ADAR2*$^{flox/flox}$ mice with VAChT–Cre.Fast mice to obtain AR2 mice.

AR2 mice. Intercrosses of *ADAR2*$^{flox/+}$/VAChT–Cre.Fast mice produced *ADAR2*$^{flox/flox}$/VAChT–Cre.Fast (AR2) mice, either heterozygous or homozygous for the Cre transgene, which directs restricted Cre expression under the control of the vesicular acetylcholine transporter gene promoter in a subset of cholinergic neurons, including the spinal motor neurons (Misawa et al., 2003). Cre expression levels were found not to differ in mice heterozygous or homozygous for the VAChT–Cre.Fast transgene (Misawa et al., 2003). The same intercrosses also produced, as littermates of AR2, *ADAR2*$^{flox/flox}$ (Ctl1) and *ADAR2*$^{+/+}$/VAChT–Cre.Fast mice (Ctl2), which were used as controls. Both genders of AR2 and control mice were used, but littermates heterozygous for the floxed ADAR2 allele were not used in this study. All genotyping was performed by PCR on DNA from tail biopsies. PCR primers and amplicon sizes for the different alleles are listed in supplemental Table S1 (available at www.jneurosci.org as supplemental material).

AR2/GluR-B$^{R/R}$ *mice.* AR2/GluR-$B^{R/R}$ mice were generated by intercrossing ADAR2$^{flox/+}$/VAChT–Cre.Fast/GluR-$B^{R/+}$ mice, which had been produced by crossbreeding AR2 mice with GluR-$B^{R/R}$ mice. The AR2/GluR-$B^{R/R}$ mice used by us were either heterozygous or homozygous for the Cre transgene (Misawa et al., 2003) and homozygous for the floxed ADAR2 and the GluR-B(R) allele. The desired genotype was found approximately once in every 20 offspring. Other genotypes produced by the intercrosses were not used in this study. All genotyping for the ADAR2 and GluR2 (GluR-B) alleles as well as for the Cre transgene was by PCR on DNA extracted from tail biopsies. PCR primers and amplicon sizes for the different alleles are listed in supplemental Table S1 (available at www.jneurosci.org as supplemental material).

Genomic PCR and reverse transcription-PCR. Genomic DNA was extracted from mouse tails using the High Pure PCR Template Preparation kit (Roche). Total RNA was isolated from brain and spinal cord tissue, and first-strand cDNA was synthesized and then treated with DNase I (Invitrogen) as described previously (Kawahara et al., 2003b). Primer pairs and the conditions used for PCR are presented in supplemental Table S1 (available at www.jneurosci.org as supplemental material). Positions of primer pairs used for genomic ADAR2 PCR (Fig. 1*A*, F1/R1) and ADAR2 reverse transcription (RT)-PCR (Fig. 1*C*, F2/R2) are indicated.

Analysis for editing efficiency at A-to-I sites. Editing efficiencies at the Q/R sites in GluR2 mRNAs were calculated by quantitative analyses of the digests of RT-PCR products with BbvI as described previously (Takuma et al., 1999; Kawahara et al., 2003a, 2004). In brief, 2 μl of cDNA were subjected to first PCR in duplicate in a reaction mixture of 50 μl containing 200 mM each primer, 1 mM dNTP Mix (Eppendorf), 5 μl of 10× PCR buffer, and 1 μl of Advantage 2 Polymerase mix (Clontech). The PCR amplification began with a 1 min denaturation step at 95°C, followed by 40 cycles of denaturation at 95°C for 10 s, annealing at 60°C for 30 s, and extension at 68°C for 40 s. Nested PCR was conducted on 2 μl of the first PCR product under the same conditions with the exception of the annealing temperature (58°C). Primer pairs used for each PCR were listed in supplemental Table S1 (available at www.jneurosci.org as supplemental material). After gel purification using the Zymoclean Gel DNA Recovery kit according to the protocol of the manufacturer (Zymo Research), an aliquot (0.5 mg) was incubated with BbvI (New England Biolabs) at 37°C for 12 h. The PCR products originating from Q/R site-edited GluR2 mRNA had one intrinsic restriction enzyme recognition site, whereas those originating from unedited mRNA had an additional recognition site. Thus, restriction digestion of the PCR products originating from edited GluR2 mRNA should produce different numbers of fragments (two bands at 219 and 59 bp) from those originating from unedited GluR2 mRNA (three bands at 140, 79, and 59 bp). Because the 59 bp band would originate from both edited and unedited mRNA but the 219 bp band would originate from only edited mRNA, we quantified the molarity of the 219 and 59 bp bands using the 2100 Bioanalyzer (Agilent Technologies) and calculated the editing efficiency as the ratio of the former to the latter for each sample (supplemental Table S1, available at www.jneurosci.org as supplemental material).

With similar methods, we calculated the editing efficiencies at the Q/R sites in GluR5 and GluR6 mRNA and in GluR2 pre-mRNA, the R/G site in GluR2 mRNA, and the I/V site in Kv1.1 mRNA (Paschen et al., 1994; Takuma et al., 1999; Kawahara et al., 2003a, 2004; Nishimoto et al., 2008). The following restriction enzymes were used for restriction digestion of the respective A-to-I sites: BbvI for the Q/R sites, MfeI (New England Biolabs) for the I/V site, and MseI (New England Biolabs) for the R/G site. Primer pairs used for each PCR and sizes of restriction digests of PCR products were indicated in supplemental Table S1 (available at www.jneurosci.org as supplemental material).

Behavioral analyses. Using a mouse-specific rotarod (SN-445; Neuroscience Corp.), we determined the maximal time before falling at 10 rpm during a 180 s period; each run consisted of three trials. Grip strength was measured with a dynamometer (NS-TRM-M; Neuroscience Corp.). Measurements were conducted weekly by a researcher blind to genotype and age of the mice.

Isolation of single motor neurons and brain tissue. Single-cell isolation from frozen spinal cord tissue was performed with a laser microdissection system (Leica AS LMD; Leica Microsystems) as described previously (Kawahara et al., 2003b, 2004). All of the large motor neurons (diameter larger than 20 μm) in the anterior horn were dissected from 14-μm-thick cervical cord sections, and three neurons each were collected together into respective single test tubes containing 200 μl of TRIZOL Reagent. In addition, using the same method, nuclei of oculomotor nerve and of facial nerve were dissected from the brainstem sections of AR2 mice and control mice at 12 months of age. The positions of these cranial nerve nuclei were identified using the Paxinos and Franklin mouse brain atlas (Paxinos and Franklin, 2001). All samples were kept at −20°C until use.

Immunohistochemistry. Under deep anesthesia with isoflurane, mice were transcardially perfused with 3% paraformaldehyde and 1% glutaraldehyde in PBS. The brains and spinal cords were removed and immersed in serially increasing concentrations of a sucrose–PBS solution (final sucrose concentration of 30%). The immunohistochemical procedure was performed on 10-μm-thick sections, which were cut with a cryostat (model HM500 O; Microm). The sections were analyzed with a

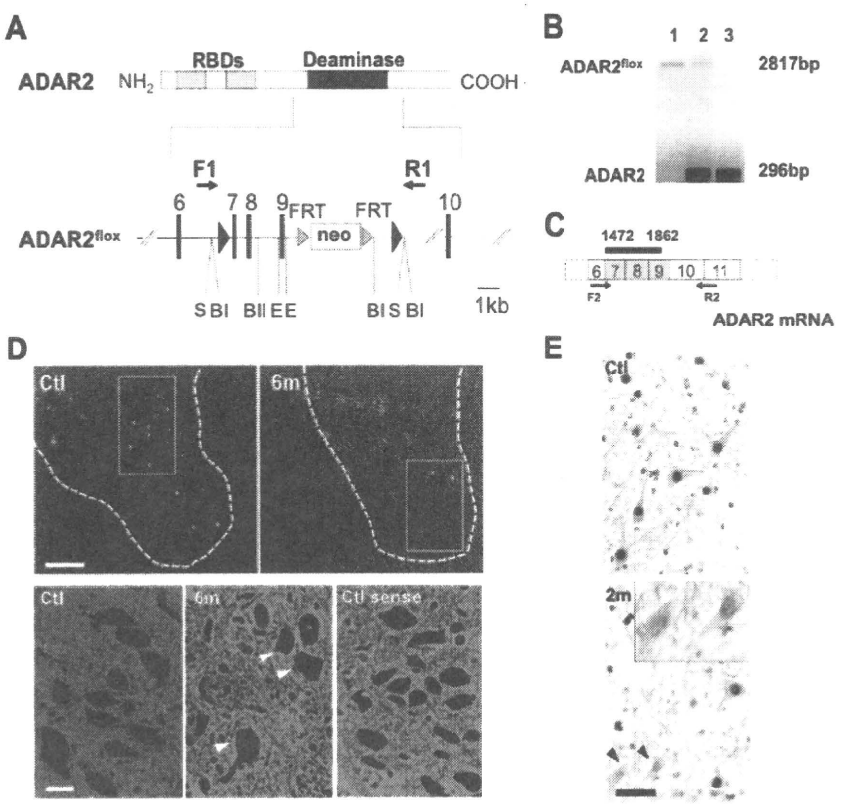

Figure 1. Generation of a conditional ADAR2 knock-out mouse. ***A***, A LoxP site (filled triangle) was inserted into intron 6 and another LoxP site in intron 9 with a selection cassette containing the gene for neomycin resistance (Neo) flanked by FRT sites. Exons are depicted as black bars with numbers. RBDs, RNA binding domains; F1/R1, primer pair (supplemental Table S1, available at www.jneurosci.org as supplemental material) for ***B***; S, SfiI; BI, BglI; BII, BglII; E, EcRI. ***B***, Genomic PCR using template DNA obtained from the tails of *ADAR2*$^{flox/flox}$ mice (lane 1), *ADAR2*$^{flox/+}$ mice (lane 2), and *ADAR2*$^{+/+}$ mice (lane 3). ***C***, Exons excised by recombination are shown as shaded areas in the mRNA, and a black bar indicates the *in situ* hybridization probe (supplemental Table S1, available at www.jneurosci.org as supplemental material) for ***D***. F2/R2, Primer pair (supplemental Table S1, available at www.jneurosci.org as supplemental material) used in Figure 2 ***B***. ***D***, *In situ* hybridization using a probe that encompasses the region excised by Cre-mediated recombination. There is a large number of punctate signals in the gray matter (outlined with dotted lines) of control mice (Ctl), whereas nuclei of some large neurons in the anterior horn were devoid of signal in the *ADAR2*$^{flox/flox}$/VAChT–Cre.Fast (AR2) mice at 6 months of age (6m; arrowheads in magnified view). The sense probe did not yield a visible signal in the control mice at the same age (Ctl sense). Scale bars: top panels, 200 μm; bottom panels, 25 μm. ***E***, All SMI-32-positive large neurons in the anterior horn (AHCs, brown color in the cytoplasm) of the cervical cord (C5) were ADAR2 positive (dark gray color in the nuclei) in the control mice (Ctl), whereas some of them were devoid of ADAR2 immunoreactivity in AR2 mice at 2 months of age (2m, arrowheads and inset). Sections were counterstained with hematoxylin. Scale bar: 50 μm; inset, 25 μm.

standard avidin–biotin–immunoperoxidase complex method using the M.O.M. Immunodetection kit (Vector Laboratories) for mouse primary antibodies and Vectastain ABC IgGs (Vector Laboratories) for other primary antibodies. The following primary antibodies were used: mouse anti-nonphosphorylated neurofilament H (SMI-32; dilution at 1:1000; Covance), mouse anti-neuronal nuclei (NeuN) (dilution at 1:500; Millipore Bioscience Research Reagents), sheep anti-rat RED1 (ADAR2) N terminus [dilution at 1:500; a gift from Dr. R. B. Emeson (Sansam et al., 2003)], rabbit anti-glial fibrillary acidic protein (GFAP) (dilution at 1:200; Lab Vision), and rat anti-mouse MAC-2 (dilution at 1:500; Cedarlane). Color was developed with the HRP–DAB System (Vector Laboratories).

Muscles and neuromuscular junctions. Medial gastrocnemius muscles and medial quadriceps muscles were dissected, pinned in mild stretch, and mounted on cork blocks and were quickly frozen in isopentane–liquid nitrogen. Samples were stored at −80°C until use. Five-micrometer-thick transverse frozen sections were stained with hematoxylin and eosin. Twenty-micrometer-thick frozen longitudinal sections were stained with tetramethylrhodamine–bungarotoxin. The same section was incubated with monoclonal antibodies to neurofilament (NF160; dilution at 1:200; Millipore Bioscience Research Reagents) and synaptophysin (dilution at 1:100; Cell Signaling Technologies) and then with Alexa Fluor 488 rabbit anti-mouse IgG (dilution at 1:100; Invitrogen) as the secondary antibody. Stained sections were examined under an LSM-510 confocal microscope system (Carl Zeiss).

Electrophysiology. Mice were anesthetized with isoflurane and placed in a prone position on a thermal pad at 37°C for the examination. Electromyogram (EMG) recordings using a Power Lab 26T and EMG machine (AD Instruments) were obtained using a 29-gauge, Teflon-coated, monopolar needle electrode. The recording electrode was inserted into the gastrocnemius muscles, and spontaneous electrical activity was recorded for 120 s using a Lab Chart analysis system (AD Instruments).

Morphological observation and stereology. Sections of the fifth cervical (C5) and fifth lumbar (L5) spinal cord segments were sequentially immunostained with RED1 and SMI-32 using the HRP–DAB system with and without the addition of $NiCl_2$ for color development. Some sections were immunostained with NeuN. ADAR2-positive and -negative neurons were separately counted among SMI-32-positive neurons with diameters larger than 20 μm in 10 sections for each mouse. The number of NeuN-positive neurons with diameter smaller than 20 μm in the ventral gray matter (ventral to the line running though the ventral edge of the central canal) was counted in 10 C5 sections for each mouse at 12 months of age. None of the NeuN-positive small neurons exhibited SMI-32 or GFAP immunoreactivity. The entire brainstem of each mouse at 12 months of age was cut axially to produce a 10-μm-thick section, and the numbers of all the neurons with nucleoli in the nuclei of cranial motor nerves were counted under a light microscope after cresyl violet staining. The position of each nucleus was stereologically determined using a mouse brain atlas (Paxinos and Franklin, 2001). The positions from the bregma were from −3.80 to −4.24 mm (nucleus of oculomotor nerve), from −4.36 to −4.48 mm (nucleus of trochlear nerve), from −4.84 to −5.34 mm (motor nucleus of trigeminal nerve), from −5.52 to −5.80 mm (nucleus of abducens nerve), from −5.68 to −6.48 mm (nucleus of facial nerve), from −7.08 to −7.92 mm (dorsal nucleus of vagus nerve), and from −7.08 to −8.12 mm (nucleus of hypoglossal nerve). The density of neurons in each nucleus was estimated by dividing the total number of neurons in each nucleus by the volume of the nucleus, which was calculated as the product of the area of the nucleus and the thickness of each section. In addition, transverse, 1-μm-thick, Epon-embedded sections of the anterior horns of the spinal cord, and the ventral roots at the L5 level were prepared and stained with 0.1% toluidine blue. Cell counting was performed by researchers who were blind to the genotype of the mouse.

In situ *hybridization.* Anesthetized mice were perfusion fixed with Tissue Fixative (GenoStaff). Dissected cervical cord tissues were sectioned after they were embedded in paraffin. Antisense and sense *adarb1* cRNA probes (Fig. 1*C*) (supplemental Table S1, available at www.jneurosci.org as supplemental material) were generated from the mouse *adarb1* open reading frame sequence, which was cloned into the pGEMT-Easy vector (Promega). Digoxigenin-labeled cRNA probes were prepared with the DIG RNA Labeling mix (Roche Applied Science). Color was developed with nitro blue tetrazolium/5-bromo-4-chloro-3-indolyl phosphate, and tissue sections were counterstained with Kernechtrot stain solution

(Muto Pure Chemicals). After mounting, 24-bit color images were acquired by scanning of the sections. Digoxigenin signals were isolated by uniformly subtracting the counterstaining color component using Photoshop version 9.0.2 (Adobe Systems) (Ohmae et al., 2006; Takemoto-Kimura et al., 2007).

Statistics. Differences in behavior and survival rates between groups were analyzed using log-rank analysis with SPSS software (version 15; SPSS Inc.), and GraphPad Prism version 4 (GraphPad Software), respectively. The differences in neuronal number between each group and the control samples were examined with a repeated-measures ANOVA. The SPSS version 15 software was used for ANOVA, followed by a Tukey–Kramer statistical test.

Results

Generation of the *ADAR2*$^{flox/flox}$/VAChT–Cre mouse, designated as AR2 mouse

We constructed the mouse *ADAR2*^{flox} allele by flanking exons 7–9 of the *adarb1* gene (mouse *ADAR2* gene) with loxP sites (Fig. 1*A*) (supplemental Table S1, available at www.jneurosci.org as supplemental material). Exons 7–9 encode the majority of the adenosine deaminase motif in the *adarb1* gene (Feng et al., 2006), and Cre-mediated deletion of this region ablates ADAR2 activity. To ablate ADAR2 activity selectively in motor neurons, we crossed *ADAR2*$^{flox/flox}$ mice with VAChT–Cre.Fast mice. In VAChT–Cre.Fast mice, Cre expression is under the control of the vesicular acetylcholine transporter gene promoter, which is active in cholinergic neurons, including spinal motor neurons (Misawa et al., 2003). In these transgenic mice, Cre expression is developmentally regulated, and ~50% of motor neurons express Cre by 5 weeks of age, independent of the heterozygous or homozygous state of the transgene (Misawa et al., 2003). The resulting *ADAR2*$^{flox/flox}$/VAChT–Cre.Fast mice, referred to here as AR2 mice (for breeding, see Materials and Methods), therefore would lack ADAR2 activity in a subset of motor neurons in the spinal cord and other brain motor nuclei after expression of Cre by 5 weeks of age. *In situ* hybridization with a probe encompassing the sequence excised by Cre-mediated recombination (Fig. 1*C*) demonstrated that several large neurons in the anterior horn (AHCs) were devoid of *adarb1* gene signal in the AR2 mice, whereas all the AHCs exhibited the signal in control littermates (Fig. 1*D*). Similarly, a subset of the AHCs were devoid of ADAR2 immunoreactivity in AR2 mice, whereas all AHCs exhibited ADAR2 immunoreactivity in the controls (Fig. 1*E*). There was no difference in the results on male and female AR2 mice.

ADAR2 activity in ADAR2-null motor neurons

Next we examined the effects of recombination of the *ADAR2*^{flox} allele on ADAR2 activity. We dissected all large neurons in the anterior horn (AHCs) (for AHC identification, see supplemental Fig. S1*A*, available at www.jneurosci.org as supplemental material) from frozen sections from 2-month-old AR2 mice ($n = 4$) using a laser microdissector (Fig. 2*A*). We verified that these AHCs, but not small neurons in the anterior horn, are the spinal motor neurons by RT-PCR for choline acetyltransferase on a single-cell lysates (supplemental Fig. S1, available at www.jneurosci.org as supplemental material). Because RT-PCR of GluR2 mRNA on the lysates of three neurons, but not the lysates of one or two motor neurons, reproducibly yielded amplification products, we analyzed the extent of GluR2 Q/R site editing on RNA extracted from the lysates of three pooled AHCs (designated as a specimen) by quantitative analysis of the BbvI-restriction digests of the RT-PCR products, as described previously (Kawahara et al., 2003b, 2004). Among 116 specimens examined, eight showed 0% and 42 showed 100% Q/R site editing, with the remaining 66 specimens distributed between the ranges of 17 and 98% (Fig. 2*A*) (supplemental Table S2, available at www.jneurosci.org as supplemental material). Because AHCs of control littermates (these carried wild-type ADAR2 alleles or no Cre transgene; see Materials and Methods) expressed only edited GluR2 mRNA, the presence of samples exhibiting 0% Q/R site editing suggests that ADAR2-expressing neurons expressed only edited GluR2 mRNA, whereas ADAR2-null neurons expressed only unedited GluR2 mRNA. Then, DNA and total RNA from the specimens were collected in four different groups according to the proportions of unedited GluR2 (Fig. 2*A*). Using PCR, we demonstrated that the samples with 100% editing efficiency (group 0:3) harbored the truncated *ADAR2*^{flox} gene and Cre transcripts, whereas the samples with 100% editing efficiency (group 3:0) carried the full-length *ADAR2*^{flox} gene and did not express Cre (Fig. 2*B*). Those samples with both edited and unedited GluR2 mRNA (groups 1:2 and 2:1) exhibited both full-length and truncated ADAR2 along with the Cre transcript. These qualitative results are consistent with the assumption that recombination of the *ADAR2*^{flox} alleles occurred in a Cre-dependent manner and that this recombination abolished the editing of the GluR2 Q/R site. Among other A-to-I sites examined, we found a significant reduction in editing efficiency only at the GluR6 Q/R site (supplemental Table S3, available at www.jneurosci.org as supplemental material).

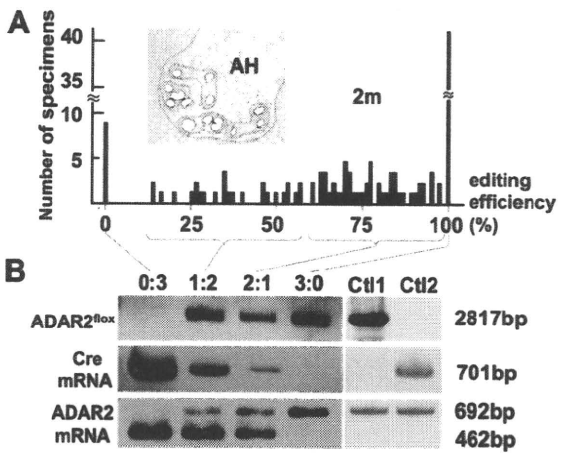

Figure 2. Cre-dependent targeting of ADAR2 and GluR2 Q/R site-editing in motor neurons. ***A***, Frequency histogram of editing efficiency at the GluR2 Q/R site in specimens (lysates containing 3 motor neurons) obtained from AR2 mice at 2 months of age (2m; $n = 4$). Neurons were dissected with a laser microdissector (inset). ***B***, Specimens ($n = 116$) were collected into four groups depending on the predicted number of ADAR2-deficient neurons in each specimen; the groups of specimens containing 3, 2, 1, and 0 unedited GluR2-expressing neurons were designated as groups 0:3, 1:2, 2:1, and 3:0, respectively. The *ADAR2*^{flox} gene and transcripts of the *Cre* gene and the *ADAR2*^{flox} alleles before and after recombination were analyzed for each group by PCR. AHCs expressing unedited GluR2 mRNA (group 0:3) harbored the truncated *ADAR2*^{flox} gene and Cre transcripts, whereas AHCs expressing edited GluR2 mRNA (group 3:0) carried the full-length *ADAR2*^{flox} gene and did not express Cre. Ctl1, *ADAR2*$^{flox/flox}$ mice; Ctl2, VAChT–Cre.Fast mice; AH, anterior horn of the spinal cord.

Behavioral changes

AR2 mice were hypokinetic (supplemental movie, available at www.jneurosci.org as supplemental material) and abnormal in posture (supplemental Fig. S2*A*, available at www.jneurosci.org as supplemental material), but they displayed no overt paralysis or vesico-urinary disturbances and exhibited a normal withdrawal response to noxious stimuli. They showed a lower rotarod performance than their control littermates after 5 weeks of age

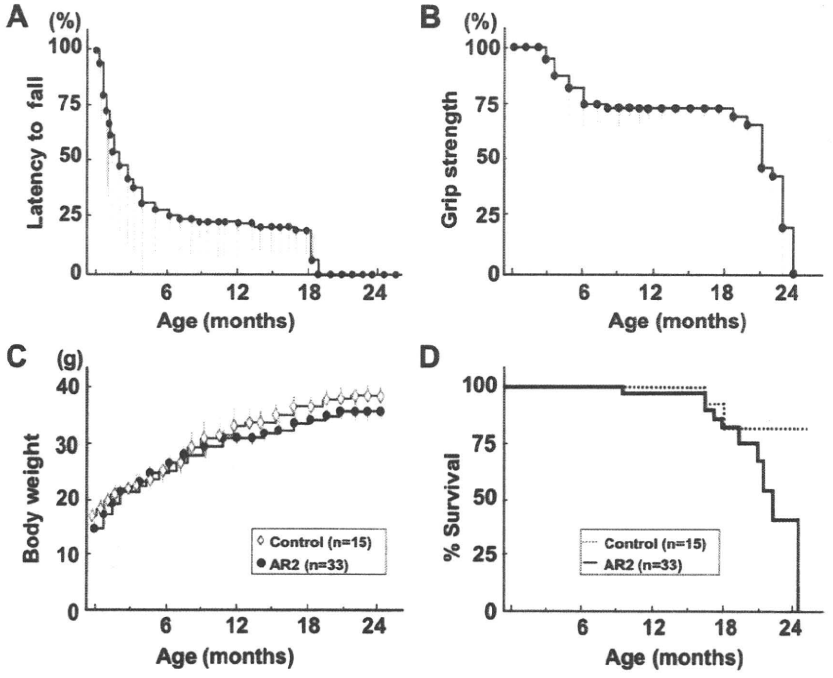

Figure 3. Behavioral changes in AR2 mice. ***A***, Rotarod performance presented as latency to fall (at 10 rpm, 180 s at the maximum) began to decline at 5 weeks of age in AR2 mice and rapidly fell to low levels during the initial 5–6 months, remaining stable until 18 months of age. Control mice exhibited full performance (180 s) until ~12 months of age, followed by slightly lower performance (>164.5 ± 6.4 s) until 24 months. ***B***, Grip strength measured declined with kinetics similar to those of rotarod performance. In ***A*** and ***B***, the scores obtained for the AR2 mice (mean ± SEM; $n = 28$) are indicated as percentage performance of control mice ($n = 15$). ***C***, AR2 mice exhibited slightly lower body weight than controls ($p > 0.05$). ***D***, AR2 mice ($n = 33$) had long lifespans, but the rate of death increased after month 18. The median ± SEM survival was 81.5 ± 16.4 weeks for AR2 mice compared with 105.1 ± 13.5 weeks for control mice ($p = 0.0262$, log-rank analysis).

(Fig. 3*A*), when the Cre expression reached the maximum level (~50% of motor neurons) (Misawa et al., 2003). Their rotarod performance rapidly declined during the initial 5–6 months of life, followed by stable performance until about 18 months of age (Fig. 3*A*). Control mice exhibited full performance (180 s) until ~12 months of age, followed by slightly lower performance (>164.5 ± 6.4 s) until 24 months. Grip strength declined with kinetics similar to those of rotarod performance (Fig. 3*B*). The AR2 mice had slightly lower body weight than the controls (Fig. 3*C*) and were relatively long-lived (81.5 ± 16.4 weeks; mean ± SEM), although not as long as control mice (105.1 ± 13.5 weeks; $p = 0.0262$, log-rank analysis) (Fig. 3*D*).

Pathological alterations in the spinal cords and muscles

Immunohistochemical examination demonstrated that all the AHCs in the spinal cord that were immunoreactive to anti-phosphorylated neurofilament antibodies (SMI-32) showed intense ADAR2 immunoreactivity in their nuclei in control mice, whereas a fraction of these cells was devoid of ADAR2 immunoreactivity in AR2 mice (Fig. 1*E*) (supplemental Fig. S2*B*, available at www.jneurosci.org as supplemental material). There were a number of degenerating AHCs with cytoplasmic vacuoles (Fig. 4*A*) and darkly stained degenerating axons in the ventral roots (Fig. 4*B*). The number of AHCs in AR2 mice markedly decreased between 1 and 2 months of age and then slowly decreased beyond 1 year of age (Fig. 4*C*). The number of ADAR2-positive AHCs in the AR2 mice decreased from 83 to 54% of the number of total AHCs in the age-matched control littermates between 1 and 2 months of age. The rapid reduction in the proportion of ADAR2-positive AHCs during this period is likely attributable to the Cre-dependent recombination of the floxed ADAR2 alleles, because the number of Cre-expressing AHCs in VAChT–Cre-.Fast mice increases developmentally until 5 weeks of age (Misawa et al., 2003). After 2 months of age, the number of ADAR2-positive AHCs did not change over the course of more than 1 year, whereas that of total AHCs decreased from 80 to 54% of the number of AHCs in the age-matched control mice (Fig. 4*C*) (Table 1). Consistent with the Cre-dependent recombination, the proportion of ADAR2-lacking AHCs in AR2 mice is in accordance with that of Cre-expressing AHCs presented in the original study of VAChT–Cre mice (Misawa et al., 2003). Concomitant with AHC degeneration, the number of myelinated axons in the ventral roots was significantly decreased (Table 1).

The kinetics of neuronal loss (Fig. 4*C*) were consistent with the kinetics of progressive motor-selective behavioral deficits (Fig. 3*A*,*B*). The long survival with hypoactivity beyond 6 months of age indicates that the remaining ADAR2-expressing neurons functioned normally during the remainder of life. The high rate of death after 18 months may reflect the failure of the remaining AHCs to compensate for an age-related decline in skeletal muscle power, including a decline in respiratory muscle strength.

We also examined denervation of skeletal muscles. Electromyography performed on AR2 mice at 12 months of age revealed fibrillation potentials and fasciculations, which are common findings in ALS, indicative of muscle fiber denervation and motor unit degeneration and regeneration (Fig. 4*D*). We observed characteristics of denervation, including muscle fiber atrophy, centrally placed nuclei, and pyknotic nuclear clumps in the skeletal muscles of AR2 mice (Fig. 4*E*). Some neuromuscular junctions (NMJs) were not innervated and other NMJs were innervated by ramified axons that innervated more than one NMJ in AR2 mice, indicating reinnervated NMJs (Fig. 4*F*). In contrast, in control mice, all the NMJs were innervated by a single axon. The proportion of denervated NMJs decreased, whereas reinnervated NMJs increased with age in AR2 mice (Fig. 4*F*). In addition, proliferation of activated astrocytes with increased GFAP immunoreactivity and of MAC2-positive activated microglial cells was detected in the anterior horns of AR2 mice (Fig. 4*G*,*H*). These results suggest that degeneration of ADAR2-lacking AHCs induced degeneration of their axon terminals, and then denervated NMJs were reinnervated by collaterally sprouted axons of ADAR2-expressing AHCs after longer survival.

Neurons in the motor nuclei of cranial nerves

The numbers of large neurons in facial and hypoglossal nerve nuclei in AR2 mice were significantly smaller than those in control mice at 12 months of age, whereas the numbers of neurons in nuclei of oculomotor nerves were not decreased (Table 1). Conversely, GluR2 Q/R site editing was significantly decreased both the in oculomotor nerve nuclei (the efficiency of GluR2 Q/R site

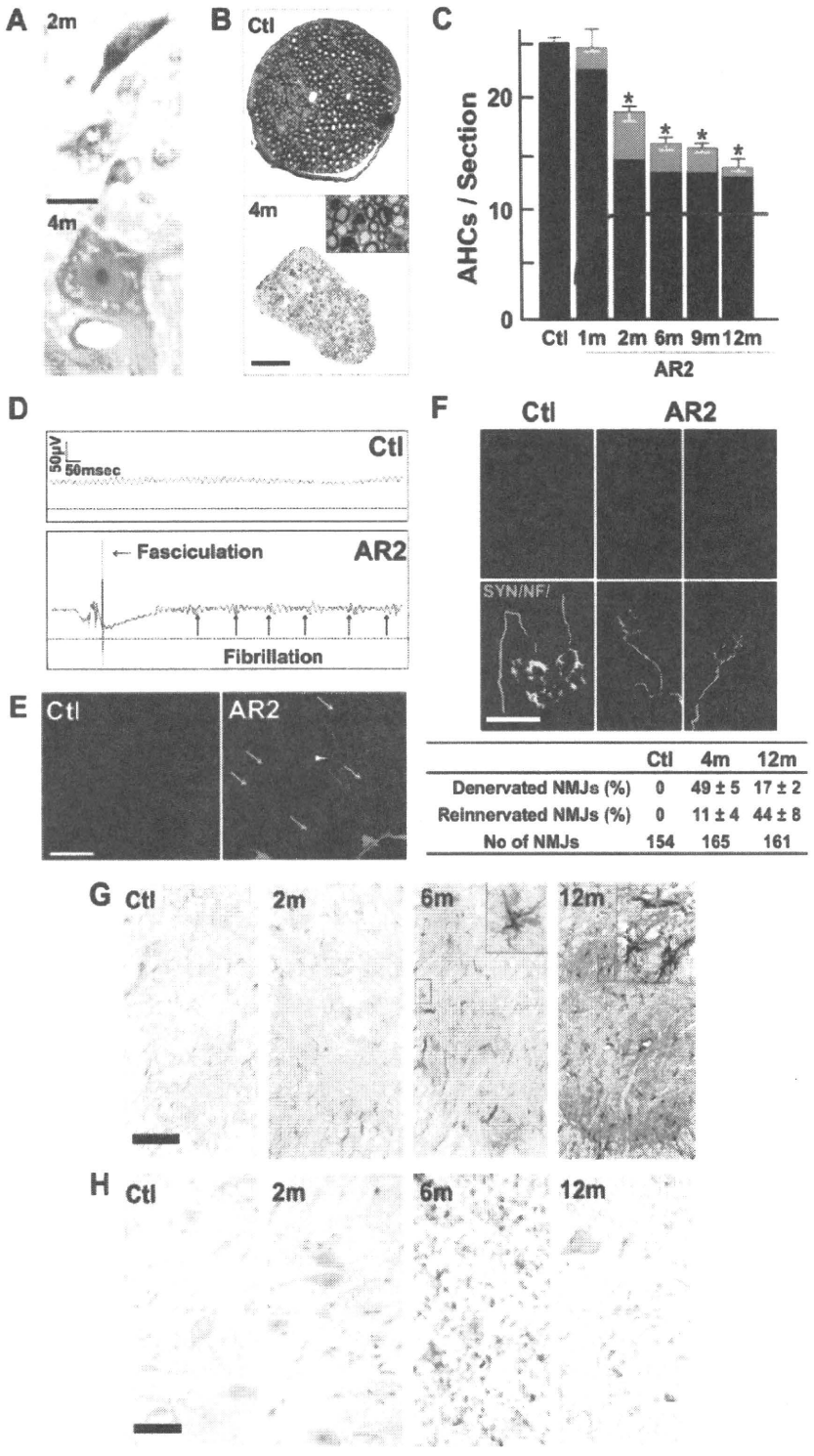

Figure 4. Loss of ADAR2-deficient motor neurons. ***A***, Degenerating AHCs in AR2 mice at 2 months (2m; Nissl staining) and 4 months (4m; toluidine blue staining, 1 μm section) of age. Scale bar: 2m, 25 μm; 4m, 12.5 μm. ***B***, Ventral root (L5) of control (Ctl) and AR2 mice at 4 months of age (4m). Inset, Magnified view of degenerating axons. Scale bar: 100 μm; inset, 20 μm. ***C***, Numbers of AHCs showing ADAR2 immunoreactivity (black columns) and lacking this immunoreactivity (gray columns) (mean ± SEM) in AR2 mice at different ages (1m, 2m, 6m, 9m, 12m). In AR2 mice, Cre expression is developmentally regulated (orange line), and ~50% of motor neurons express Cre by 5 weeks of age, with recombination of the *ADAR2* gene in ~10% of AHCs at 1 month of age and 40–45% of AHCs after 2 months of age (orange line). The number of ADAR2-lacking AHCs significantly decreased in AR2 mice after 2 months of age as a result of Cre-dependent knock-out of ADAR2 (*$p < 0.01$, repeated-measures ANOVA). The number of AHCs in the control mice did not change at different ages, and all the AHCs in controls showed ADAR2 immunoreactivity. ***D***, Electrophysiological examination in AR2 mice. Electromyography from an AR2 mouse at 12 months of age showing fibrillations and fasciculations, common findings in ALS indicative of muscle fiber denervation and motor unit degeneration and regeneration.

editing, mean ± SEM: for AR2 mice, 89.7 ± 5.8%, $n = 3$; for control mice, 100%, $n = 3$, $p = 0.0048$) and in the facial nerve nuclei (for AR2 mice, 82.6 ± 9.1%, $n = 3$; for control mice, 99.2 ± 0.2%, $n = 3$, $p = 0.0017$) of AR2 mice at 12 months of age. These results indicate that ADAR2-lacking motor neurons do not always undergo cell death, and some motor neurons, including those in the oculomotor nerve nucleus, are relatively resistant to cell death mediated by deficient ADAR2. Indeed, motor neurons innervating extraocular muscles are much less vulnerable than those innervating bulbar and limb muscles in ALS patients (Lowe and Leigh, 2002).

GluR-B^R alleles prevent motor neuron death in AR2 mice

To investigate by genetic means the role of RNA editing at the GluR2 Q/R site in the death of motor neurons, we exchanged the endogenous *GluR2* alleles in AR2 mice with GluR-B^R alleles (Kask et al., 1998), which directly encode Q/R site-edited GluR2, thus circumventing the requirement for ADAR2-mediated RNA editing. AR2/GluR-$B^{R/R}$ mice were obtained by $ADAR2^{flox/+}$/VAChT–Cre.Fast/GluR-$B^{R/+}$ mice intercrosses to generate $ADAR2^{flox/flox}$/VAChT–Cre.Fast/GluR-$B^{R/R}$ (AR2/GluR-$B^{R/R}$) mice (see Materials and Methods).

←

These findings were observed in two other AR2 mice examined but never in control mice (Ctl; $n = 2$). ***E***, Calf muscles from a wild-type mouse (left) and an AR2 mouse (middle and right) at 12 months of age. Characteristics of denervated muscles, including muscle fiber atrophy (white arrow), centrally placed nuclei, and pyknotic nuclear clumps (white arrowhead) are observed in the AR2 mouse. Hematoxylin and eosin. Scale bar, 60 μm. ***F***, NMJs and distal axons. Quadriceps muscles from a wild-type mouse (Ctl; left) and an AR2 mouse (AR2; middle and right) at 12 months of age are stained with tetramethylrhodamine–bungarotoxin (BTX) (red) and immunostained concomitantly with anti-synaptophysin and neurofilament (SYN/NF) antibodies (green). Endplates (red) were counted as "innervated" if they were merged with axon terminals (merge; yellow). Each endplate is innervated by a thick axon terminal in the Ctl mouse. In AR2 mice, in addition to the normally innervated NMJs, some NMJs were innervated by axons that simultaneously innervate more than one NMJ (reinnervated NMJs; middle), and other NMJs were devoid of axon terminals (denervated NMJs; right). More than 50 NMJs were counted in each animal in the control group and groups of AR2 mice at 4 and 12 months of age ($n = 3$ in each group). Proportions of denervated NMJs and reinnervated NMJs among total NMJs in each group are indicated as mean ± SD (percentage). Scale bar, 25 μm. ***G***, ***H***, Immunohistochemistry in the anterior horn (C5). There was a time-dependent increase in GFAP immunoreactivity (***G***) and an increase in MAC2 immunoreactivity maximal at 6 months of age (***H***) in the spinal anterior horn of AR2 mice. m, Months of age; inset, activated astroglia. Scale bars: ***G***, 100 μm; insets and ***H***, 50 μm.